Naval Research Laboratory

Washington, DC 20375-5000

NRL Memorandum Report 6779

The Charge-Exchange Neutral Problem and the Code NEUTRAL

JOHN M. LES AND ROBERT E. TERRY

Radiation Hydrodynamic Branch
Plasma Physics Division

June 26, 1991

This research was sponsored by the Defense Nuclear Agency, under Subtask Code and Title RL RB/Advanced Technology Development, Work Unite Code 00079, MIPR No. 89-565.

REPORT DOCUMENTATION PAGE

Form Approved
OMB No 0704-0188

1. AGENCY USE ONLY (Leave blank)	2. REPORT DATE	3. REPORT TYPE AND DATES COVERED
	1991 June 26	Interim

4. TITLE AND SUBTITLE

The Charge-Exchange Neutral Problem and the Code NEUTRAL

5. FUNDING NUMBERS

PE - 62715H
WU - DN880-191

6. AUTHOR(S)

John M. Les and Robert E. Terry

7. PERFORMING ORGANIZATION NAME(S) AND ADDRESS(ES)

Naval Research Laboratory
Code 4720
Washington, DC 20375-5000

8. PERFORMING ORGANIZATION REPORT NUMBER

NRL Memorandum
Report 6779

9. SPONSORING/MONITORING AGENCY NAME(S) AND ADDRESS(ES)

Defense Nuclear Agency

10. SPONSORING/MONITORING AGENCY REPORT NUMBER

11. SUPPLEMENTARY NOTES

The research was sponsored by the Defense Nuclear Agency, under Subtask Code and Title:
RL RB/Advanced Technology Development, Work Unit Code 00079, MIPR No. 89-565.

12a. DISTRIBUTION/AVAILABILITY STATEMENT

Approved for public release; distribution unlimited.

12b. DISTRIBUTION CODE

13. ABSTRACT *(Maximum 200 words)*

The code named NEUTRAL was developed to simulate the problem of charge-exchange neutrals, which has been proposed to explain the anamolous gap closure in a Reflex Switch. NEUTRAL is one dimensional in position and velocity space and includes a static external electric field. Monte Carlo techniques are used to model the charge-exchange process. Analytic expressions are derived using the one dimensional Boltzmann equation, assuming a constant charge-exchange cross section, and they are compared against the NEUTRAL simulation runs. Good agreement is found between the two results. Some parameters were also varied independently to test the response of NEUTRAL. It was found that the code gives reasonable answers for a wide range of the input. From these benchmark tests it is concluded that NEUTRAL is operating correctly.

14. SUBJECT TERMS

Reflex switch
Charge exchange

15. NUMBER OF PAGES
68

16. PRICE CODE

17. SECURITY CLASSIFICATION OF REPORT	18. SECURITY CLASSIFICATION OF THIS PAGE	19. SECURITY CLASSIFICATION OF ABSTRACT	20. LIMITATION OF ABSTRACT
UNCLASSIFIED	UNCLASSIFIED	UNCLASSIFIED	SAR

CONTENTS

THE CHARGE-EXCHANGE NEUTRAL PROBLEM AND THE CODE NEUTRAL

Introduction

In this report we will discuss the theoretical aspects and the computer modeling of the charge-exchange neutral process. Such a mechanism has been proposed to explain the premature gap closure in pulsed power ion diodes[1] as well as in the Reflex Switch[2]. In the reflex switch it is important that we understand this anamolous gap closure, since such an event causes reduced power to the load[3]. In the presentation below we briefly review the operation of the reflex switch[4] and then we will discuss the analytical model for charge-exchange. We then will present some results from a monte carlo simulation code.

Reflex Switch

The closed mode of the reflex switch can be seen in figure 1 . An anode foil, denoted here in the text by A, is set between the primary cathode K1 and the electrically floating secondary cathode K2. There is also an applied axial magnetic field B_z, which we will not concern ourselves with here. In the closed mode of the switch, electrons emmitted from K1 are repelled by the potential in the A-K2 gap, causing the electrons to repeatedly traverse (reflex) through the anode foil. From the resulting anode plasma an ion current is drawn, as shown in the figure. As these ions are accelerated through the partially ionized anode plasma, they can charge-exchange, creating a flux of energetic neutrals into the gap. The neutrals, by electrical breakdown, then cause an impedance collapse in the anode-cathode gap[1]. This is the model of neutral-charge exchange as mentioned in the introduction. The anode-K2 gap spacing determines when the switch opens, and it is supposedly plasma motion that causes this gap to short and stops the electrons from reflexing[4]. It is also possible that neutrals can be filling this gap as well, making the switch open prematurely[2]. We will now go into more detail on the neutral charge-exchange problem as given below.

Manuscript approved August 31, 1989.

Neutral Charge-Exchange Model

Prono et al.[1] were the first to suggest that premature gap closure was caused by neutrals that were produced from ions charge-exchanging in a background medium. The physical model they used is given in figure 2. There is an ion flux at x = 0 into a partially ionized plasma, which contains mostly neutrals at a uniform density n_A. The ions charge-exchange as they are accelerated through the neutral gas, by the constant electric field E. In the microscopic picture of the charge-exchange process, an ion, given by the "+", picks up an electron from a similiar type atom(s), producing an energetic neutral n with the same velocity as the incident ion and an ion with zero speed. We note that this newly born ion will then gain energy from the field E, and can charge-exchange as well. Thus one ion can produce many neutrals. The flux of neutrals into the vacuum gap, given by $G(x=x_{max})$, is the cause of the gap closure. The physical model of the charge-excahnge process, as given here, can be described analytically and is presented below.

To find the neutral flux, we follow the analysis given by Prono et al.[1]. Assuming the problem described above is in a steady state we can solve for the ion distribution function f(x,v) and the neutral distribution function g(x,v) by starting with the one dimensional Boltzmann equation given by

$$v\frac{\partial f}{\partial x} + \frac{qE}{m}\frac{\partial f}{\partial v} = -n_A\sigma f + \delta(v-\varepsilon)\int_0^\infty dv' n_A \sigma' v' f' \qquad (1)$$

$$v\frac{\partial g}{\partial x} = n_A \sigma v f \qquad (2)$$

where,

f(v,x)dxdv = number of ions (per unit area) in the phase volume dxdv

g(x,v)dxdv = number of neutrals (per unit area) in the phase volume dxdv

q = charge of the interacting ion

m = mass of the ion

E = electric field

n_A = neutral background density

v = velocity in x direction

σ = charge exchange cross section, which in general depends on v

By σ' and f' in equation (1), we mean $f' = f(v',x)$ and $\sigma' = \sigma(v')$. Also in (1) we have assumed that v is always greater than zero (no reverse flow), and initially, we assume that the slow ion produced in the charge-exchange process has a very small energy. This is the meaning of the ε term in the argument of the Dirac delta function. So the first term on the right hand of equation (1) is the loss of ions due to charge-exchange, while the second term denotes ion production. While in equation (2) we see that the neutrals are not affected by the electric field, and that $n_A \sigma f$ is the neutral production rate. Also note that in the above equations, as well as in our model in general, we have ignored the ionization of the fast neutrals as they pass through the background medium. Steady state conditions imply that the flux of ions is a constant, which we and Prono et al. denote as F. Thus we can write, assuming the ions are born with small velocity ε,

$$F = \int_0^\infty dv v f(v,x) \qquad (3)$$

$$f(v,x=o) = \frac{F}{\varepsilon}\,\delta(v-\varepsilon) \qquad (4a)$$

$$g(v,x=o) = 0 \qquad (4b)$$

where (3) is just the usual definition of the flux, and equation (4a) is the assumed ion distribution at the injection point. The quantity ε is used to avoid mathematical ambiguities later on in the analysis and will eventually be set to zero[1]. Equation (4b) states that there are no neutrals created at the injection point. We can Laplace

transform equations (1) and (2), using the boundary conditions (4a) and (4b), to find

$$\frac{\partial \bar{f}}{\partial w} + \frac{1}{qE}(p+n_A\sigma)\bar{f} = \frac{\delta(w-\varepsilon)mF}{qE}\left(1 + \int_o^\infty dw' \frac{n_A\sigma' f'}{mF}\right) \qquad (5)$$

$$\bar{g} = \frac{n_A\sigma f}{p} \qquad (6)$$

with the usual definition of the Laplace transform being,

$$\bar{f} = f(w,p) \equiv \int_o^\infty dx\, e^{-px} f(w,x)$$

Note that in equations (5) and (6) we have used a change of variable, where w is the kinetic energy, $w = mv^2/2$. Solving for $\bar{f}$, after some integrations of equation (5), see Appendix A, we find

$$\bar{f}(w) = f(w,p) = \frac{mF}{p} H(w) \frac{e^{-\int_o^w \frac{1}{qE}(p + n_A\sigma')dw'}}{\int_o^\infty dw\, e^{-\int_o^w \frac{1}{qE}(p + n_A\sigma')dw'}}$$

$$H(w) = \begin{cases} 1 & \text{for } w > 0 \\ 0 & \text{for } w < 0 \end{cases} \qquad (7)$$

where H(w) is the usual Heaviside step function and we have let ε go to zero. From equations (7) and (6) we see that once we have the functional form of the charge-exchange cross section σ, we can in principle determine the ion and neutral distribution functions by inverse Laplace transform. However, one can see that in general, exact solutions will be very difficult, if not impossible, to obtain. At this point we diverge from the analysis of Prono et al., and we assume that σ, the charge-exchange cross section, is constant for all w. Even though this assumption is less physical than having a cross section that decreases with energy, as Prono et al. did[1], we can at

least obtain closed analytical expressions for f and g. We note here that if the average ion energy is much less than the "cut off energy" of the cross section, again see reference (1), then a constant cross section is a good approximation. Returning to the problem at hand, using equations (6) and (7) with σ being a constant, we find by inverse Laplace transform that the distribution functions f and g are given by

$$f(w,x) = \frac{mF}{qE} e^{-\frac{w}{qE\lambda}} \left[\delta\left(x - \frac{w}{qE} \right) + \frac{1}{\lambda} H\left(x - \frac{1}{qE} \right) \right] \qquad (8)$$

$$g(w,x) = \frac{mF}{qE\lambda} e^{-\frac{w}{qE\lambda}} H\left(x - \frac{w}{qE} \right) \left[1 + \frac{1}{\lambda}\left(x - \frac{w}{qE} \right) \right] \qquad (9)$$

where $\lambda = 1/n_A\sigma$, which is the mean free path for charge-exchange. As before, H is the Heaviside step function as defined in equation (7), and δ is the usual Dirac delta function. Taking various moments of the distribution functions, we find

$$\int_0^\infty vf(v,x)dv = \int_0^\infty f(w,x)\frac{dw}{m} = F \qquad (10)$$

$$\Gamma_n(x) = \int_0^\infty g(w,x)\frac{dw}{m} = F\cdot\left(\frac{x}{\lambda} \right) \qquad (11)$$

$$F_w(x) = \int_0^\infty wf(w,x)\frac{dw}{m} = F\cdot(qE\lambda)\left(1 - e^{-(x/\lambda)} \right) \qquad (12)$$

$$G_w(x) = \int_0^\infty wg(w,x)\frac{dw}{m} = F\cdot(qE\lambda)\left((e^{-(x/\lambda)} - 1) + (x/\lambda) \right) \qquad (13)$$

Equation (10) is just a verification of equation (3). $\Gamma_n(x)$ is the neutral flux profile, which for our case happens to be linear. $F_w(x)$ and $G_w(x)$ are the ion and neutral energy fluxes, respectively. Notice that the term, $qE\lambda$, keeps appearing in our equations. This is just the average energy an ion gains before charge-exchanging. Defining the mean particle energy as Prono et al. does[1], we find

$$\langle E_i \rangle = \frac{F_w}{F} = (qE\lambda)\left(1 - e^{-(x/\lambda)} \right) \qquad (14)$$

$$\langle E_n \rangle = \frac{G_w}{\Gamma_n} = (qE\lambda)\left[\left(\frac{\lambda}{x} \right)\left(e^{-(x/\lambda)} - 1 \right) + 1 \right] \qquad (15)$$

and in both cases, as $x \to 0$, both $\langle E_i \rangle$ and $\langle E_n \rangle$ go to zero, as one would expect. For $x \to \infty$, both expressions go to the value $qE\lambda$. The analytical solutions (10) through (15) are very useful in benchmarking a computer simulation of this neutral charge-exchange model. In the next section we will compare (9), (10), (11), and (15) to the results from a computer code named NEUTRAL.

Computer Simulation and Modeling

The code NEUTRAL was developed to model the charge-exchange problem as mentioned in the previous section, and is the final member in a series of codes which varied in their degree of complexity. The first code that was written was designed to simulate ions interacting with a background medium with no applied electric field and no time dependence. The second code in the series included ion charge-exchanging in an applied electric field, but the model was still time independent. The final member, NEUTRAL, includes all ot the capabilities of the previously mentioned codes, and is time dependent.

NEUTRAL uses Monte Carlo techniques to model the charge-exchange process, and the code was written so that either applied or self-consistent electric fields can be used. This second field mode however, has not been tested yet. Our main concern was to model the problem as envisioned by Prono et al.[1], since experimental measurements of relevant quantities, such as densities and electric fields, are practically nonexistent. The code works by imitating the problem as pictured in figure 2. Ions are injected at the left hand boundary and then an electric field is determined. Next the particles are moved in position and velocity space. Then the code decides wether or not a given ion undergoes charge-exchange. This is done by randomly generationg a number between 0 and 1, and then comparing it

to $e^{-\Delta L/\lambda}$, where ΔL is the distance traveled by the particle in a given time step. As before, λ is the mean free path for charge-exchange. If the random number is greater than $e^{-\Delta L/\lambda}$ a charge-exchange event event is said to have occurred, and in the fast ions place, a fast neutral with the same velocity is created and tracked, while another ion is created with zero speed. One can see that this method assumes that an ion interacts only once in a given time step, which is valid if $\Delta L \ll \lambda$. This method is also well suited for the case where λ depends on x and w, through $n_A = n_A(x)$ and $\sigma = \sigma(w)$. So to summarize NEUTRAL, for every time step, ions are injected, electric fields are computed, particles are pushed in x and v, and charge-exchange events are randomly generated. We now will present some of the output from the code NEUTRAL in the next section.

Simulation Results

As mentioned earlier we are using the problem posed by Prono et al.[1], assuming the charge-exchange cross section σ is a constant in energy, to benchmark the code NEUTRAL. We used protons as our ion source and had hydrogen as our background gas. Some of the physical parameters assumed in this standard (reference) case were

$$n_A = 1.0 \times 10^{16} \text{ / cm}^3$$
$$E = 1 \text{ MV/cm} \simeq 3.333333 \times 10^3 \text{ statvolts/cm}$$
$$q = 4.8032 \times 10^{-10} \text{ statcoulombs}$$
$$\sigma = 2.0 \times 10^{-15} \text{ cm}^2$$
$$m = 1.6726 \times 10^{-24} \text{ g}$$
$$x_{max} = 0.1 \text{ cm}$$

thus,

$$\lambda = 5 \times 10^{-2} \text{ cm}$$

and

$$N_{inj} = 500$$
$$NTS = 400$$
$$\Delta t = 1.136 \times 10^{-11} \text{ sec}$$
$$\Delta x = 5.0 \times 10^{-3} \text{ cm}$$

The quantity m is the ion mass, which for this case is just the proton mass, and q is the charge of the proton. From the above input parameters it would not be surprising if we said that NEUTRAL does most of its calculations in c.g.s. units. The second set of variables N_{inj}, NTS, Δt, and Δx are, respectively, the number of ions or particles injected per time step, the number of time steps run in the simulation, the time step in seconds, and the size of the spatial mesh. The time step was chosen such that $\Delta t = \Delta x / v_{max}$, where v_{max} is the velocity of an ion if it traversed the entire charge-exchange region without interacting. The quantity x_{max} is the position of the right hand boundary, as seen in figure 2. The background neutral density, n_A, is from some mesurements made by Pal and Hammer[5]. However, this density is from a magnetically insulated diode, and not a reflex switch. We use this value of n_A because, as mentioned previously, there is no hard data on the physical parameters inside a reflex switch. In additon, see reference (1) for another estimation of the background neutral density. Now refering to figure 3, we see the code generated ion flux as a function of x, at time t = 4.54 ns (400 x 1.136×10^{-11} sec). This time is roughly two orders of magnitude greater than the mean collision time τ, estimated by

$$\tau = \lambda / \bar{v} \quad , \quad \bar{v} \simeq \sqrt{\langle E_i \rangle / m} \Big|_{x=x_{max}}$$

where $\langle E_i \rangle$ is given by equation (14). This means that we can assume that we have reached an equilibrium state. The reason the ion flux is depressed near x = 0 is due to the fact that we inject and push particles before data is collected and plotted. The dashed line is the constant ion flux F, to be used in the analytical results, equations (11), (9), and (15). Figure 4 is the code generated neutral flux profile and the dashed line is equation (11), with $F = 4.2 \times 10^{15}$ / cm^2 sec and $\lambda = 5 \times 10^{-2}$ cm. Note that we have very good agreement between theory and simulation. Figure 5 is the spatially integrated distribution of neutrals, as a function of energy in Kev, in the region $0 < x < x_{max}$. This distribution we have defined as $G_{xint}(w)$ and is given by

$$G_{xint}(w) \equiv \int_{o}^{x_{max}} g(w,x)dx =$$

$$= \frac{mF}{qE}\left(\frac{x_{max}}{\lambda}\right)\left(1 - \frac{w}{qEx_{max}}\right)\left[1 + \frac{x_{max}}{2\lambda}\left(1 - \frac{w}{qEx_{max}}\right)\right] \qquad (16)$$

Note that once again there is good agreement between the two types of results. Figure 6 is the distribution function g evaluated at $x = x_{max}$, see equation (9). Again the horizontal axis is the neutral energy in Kev. The analytical results agree well with the simulation, but there is a discrepency around 100 Kev, the maximum energy a neutral could have. One possible explanation is that such high energy neutrals are rare, so the statistics are low. Another probable situation is that due to the plotting logic, the code is missing these events that occur near the edge of the simulation space. However, figures 3 - 6 show that at least for this standard benchmark case, simulation and theory agree rather well. In addition, we note that NEUTRAL gives an average neutral energy of 25.4 Kev at $x = x_{max}$, while from equation (15) we find $\langle E_n \rangle = 28.4$ Kev. This average energy is found in NEUTRAL by numerical integration of the neutral distribution function at $x=x_{max}$, see equations (13) and (15).

To test the NEUTRAL code further we have run four additional cases. In the first two cases we changed the magnitude of the charge-exchange cross section, while keeping the rest of the input parameters the same as in the reference case, see above. While in the second case we varied the electric field E, again keeping the rest of the input parameters constant. Figures 7-10 have the same meaning as before except σ is now twice that of the standard case i.e., $\sigma = 4.0 \times 10^{-15}$ cm^2. From figure 7 we see that $F = 4.0 \times 10^{15}$ / cm^2 sec. This is slightly smaller than the flux used in the standard reference case, we will discuss this point later on. However, we notice that again we have good agreement between the analytic solutions and the simulation. More importantly these results all seem to be self consistent.

Figures 11-14 are for the case where the cross section is one half the value of the benchmark case, meaning $\sigma = 1.0 \times 10^{-15}$ cm^2. A quick calculation shows that the mean free path in this case is exactly equal to x_{max}, the width of the charge-exchange region. This is reflected by the fluctuations seen in figure 14, but even so the camparison between theory and simulation is still good. Also note from figure 13 that because $G_{xint}(w)$ is the spatial integral of the neutral distribution function, it is much smoother than $g(w,x=x_{max})$. In figures 15-18, we set the applied electric field E to one half the standard field value, while once again all the other input parameters are the same as in the reference case. From figures 17 and 18 we see that NEUTRAL underestimates the energy distributions near zero energy, by roughly 10 percent if one considers the numerical values. And since the applied field is half its original value, we of course expect that the maximum neutral energy to be half of 100 Kev, or 50 Kev. This is verified in figures 17 and 18. Figures 19-22 represent the case where we have increased the electic field strength to twice the standard value. From figure 19 we see that the ion flux is reduced by a small fraction as compared to figure 15. See also figure 7 for an addtional comparison in this slight flux decrease. Again the simulation results appear quite good. One must be aware that in general when one changes some input parameter, such as E, then one might have to modify other values, such as the time step Δt, in order to obtain reasonalble results. It seems though, from figures 7-22, that the code is stable against changes in σ and E, as long as these changes are not too large.

It seems, from the discussion of the simulation results above, that the NEUTRAL code finds its own value for the ion flux F, and for the most part this is true. But since we are supposedly in a steady state situation, the equilibrium ion flux in the charge-exchange region ($0 < x < x_{max}$) should be equal to the ion injection rate, given by

$$F = \frac{N_{inj}}{A\Delta t} \qquad (17)$$

The quantity A is an area weighting factor that is used in NEUTRAL to determine certain physical values, such as the charge density. One can see that such a factor is needed since our problem is one dimensional, but the flux and density are 2 and 3 dimensional objects, respectively. For all the cases mentioned in this study, A was set to 10^{-2} cm^2. Using N_{inj} and Δt as given in the reference case and equation (16) above, we find that theoretically, F should have the value 4.4×10^{15} / cm^2 sec. From the figures previously given we see that the code predicts ion fluxes that are at most 10 percent off from this theoretical value. We should also mention, which may be apparent at this point, that the constant ion flux read from the plots is somewhat arbitrary, but at the same time one can make a reasonable estimation of the steady state flux. The dependence of the ion flux on the variables N_{inj} and Δt, as given in equation (17), is shown in figures 23 and 27. In figure 23 the number of injected particles per time step was increased to 700, this is a factor of 1.4 times the standard case of $N_{inj} = 500$. In figure 27 we have increased the time step by a factor of two, this should reduce the flux by the same factor according to equation (17), and this is essentially the case. Notice that this same figure shows that if one increases the time step without adjusting other relevant parameters, that larger than normal fluctuations may occur in the data. The figures 24-26 and 28-30 are added here for completness only. Like before, figures 24-26 are the comparison of code results to analytic solutions for the ion flux given in figure 23, and the same goes for figures 28-30 except they are related to figure 27. From equation (17) we see that the ion flux is independent of the cross section or the electric field, or any other physical characteristic that describes the charge-exchange region. As was mentioned awhile back, we noticed a slight reduction in the steady state ion flux when the cross section or the electric field were increased by a factor of 2. This may or may not be significant. In both cases a possible general argument is that in a given spatial cell ions are being lost at a faster rate than they are injected, reducing the overall numerical flux, but this is just at first glance. However, the ion flux does not seem to vary as v_{avg}, defined as $v^2_{avg} = 2E\lambda/m$, as one may initially have guessed.

Before we continue we should mention that all of the cases considered so far, and later on as well, the ions are injected monoenergeticaly from the left hand boundary of the simulation region, with zero velocity. One can also chose to inject ions with a maxwellian distribution using NEUTRAL, if the need arises. In position space, the particles are uniformly distributed in the first spatial cell when they are injected into the system.

To see if injecting the ions with a small velocity would change our results, we used the reference case input parameters, but now each particle was given the initial velocity of 1.384×10^6 cm/sec, which corresponds to a proton at roughly 1.0 ev in temperature. The results are shown in figures 31-34, and should be compared with the standard case, figures 3-6. For the most part one can see there is no drastic changes between the two runs. Finally we will consider the case where we decreased the size of the spatial mesh cell by a factor of 0.5 from the reference standard. As one can see from figures 35, making the cells smaller produces large fluctuations in the ion flux as one would expect, but there are only small ripples in the neutral flux profile, see figure 36. In figures 37 and 38 things are relatively quiet, but this should be the case since these plots are independent of the spatial mesh cell Δx. For comparison, in figures 39-42, we doubled the size of Δx, and as expected the ion flux shows alot less fluctuations. We note that the NEUTRAL code uses only uniform mesh cells throughout the simulation region. This concludes our evaluation of the charge-exchange simulation code NEUTRAL.

Summary and Conclusions

We have found exact analytic solutions, assuming a constant charge-exchange cross section, to the one dimensional Boltzmann equation as it relates to the charge-exchange model considered by Prono et al. These results were used to benchmark the Monte Carlo code named NEUTRAL, which was written to simulate ions charge-

exchanging in a background gas. This exchange process, with the resulting flux of fast neutrals, is thought to be the cause of premature gap closure in a reflex switch. In benchmarking the NEUTRAL code we varied one input parameter while keeping the others constant. The quantities varied were, the charge-exchange cross section, the electric field, the number of particles injected, the time step, the speed of the injected particles, and the spatial mesh size. In most cases we found there was very good quantitative agreement between simulation and theory. Thus we are confident, at least for the constant electric field case, that NEUTRAL is operating correctly.

Future Work

We intend to use NEUTRAL to model problems that are more physically relevant to the charge-exchange process as it may occur in the reflex switch. Such as a cross section that varies with ion energy, a background gas density that changes with distance, and an electric field that varies in time. We will also use the results of the NEUTRAL code as input to a model, yet to be determined, of the neutral shorting mechanism inside the vacuum gap of a reflex switch.

Acknowledgements

One of the authors, J.M.L., would like to give a special thanks to John Ambrosiano for his immense help in designing the basic structure of the NEUTRAL code, and for his general guidance. Thanks must also go to Jim Geary for his input, insight, and constant support. The information and experience provided by John Creedon is greatly appreciated. Finally one of us, J.M.L, would like to thank, Paul Boris for his artistic talent in creating figure 1, and Gina Coluzzi for her help in understanding the word processor that was used to write this report.

This work was sponsored by the Defense Nuclear Agency.

REFERENCES

1. D.S. Prono, H. Ishizuka, E.P. Lee, B.W. Stallard, and W.C. Turner, J. Appl. Phys. 52, 3004 (1981).

2. J.M. Creedon, L.J. Demeter, B. Ecker, C. Eichenberger, S. Glidden, H. Helava, and G.A. Proulx, J. Appl. Phys. 57, 1582 (1985).

3. J.S. Levine, J.M. Creedon, M.Krishnan, K.D. Pearce, and P.S. Sincerny, 7th International Conference on High Power Particle Beams, Karlsruhe, July 4-8 (1988).

4. L.J. Demeter, in **Opening Switches**, ed. by, A. Guenther, M. Kristiansen, and T. Martin, (Plenum Press, N.Y., 1987).

5. R. Pal and D. Hammer, Phys. Rev. Lett. 50, 732 (1983).

6. J.M. Creedon, private communication.

7. L. Chen, private communication.

Appendix A

The solution of equation (5), is not as straight forward as one might think, so we will present the derivation here. Writing down equation (5) for convenience, we start off with,

$$\frac{\partial f}{\partial w} + \frac{1}{qE}(p + n_A\sigma)\bar{f} = \frac{\delta(w - \varepsilon)mF}{qE}\left(1 + \int_o^\infty dw' \frac{n_A\sigma'\bar{f}'}{mF} \right) \qquad (A1)$$

Creedon[6] has solved this equation by two different approaches, however we will present the derivation given more recently by Chen[7]. Multiplying equation (A1) by the integration factor

$$e^{\int_o^w \frac{1}{qE}(p + n_A\sigma')dw'}$$

and then integrating with respect to w, from 0 to w, we find

$$\bar{f}(w)e^{\int_o^w \frac{1}{qE}(p + n_A\sigma')dw'} - \bar{f}(w = o) =$$

$$= H(w - \varepsilon)e^{\int_o^\varepsilon \frac{1}{qE}(p + n_A\sigma')dw'} \cdot \frac{mF}{qE}\left(1 + \int_o^\infty dw' \frac{n_A\sigma'\bar{f}'}{mF} \right) \qquad (A2)$$

For now we assume that $\bar{f}(w=0) = 0$, and we will prove this later on. In equation (3) of the text, we apply the Laplace transform and find

$$\frac{mF}{p} = \int_o^\infty \bar{f}(w)dw \qquad (A3)$$

where we have again changed the integration variable to the energy variable w, see equation (10) . From equations (A2) and (A3) we find

$$\frac{mF}{p} = \int_0^\infty dwH(w - \varepsilon)e^{-\int_\varepsilon^w \frac{1}{qE}(p + n_A\sigma'')dw''}\left[\frac{mF}{qE}\left(1 + \int_0^\infty dw' \frac{n_A\sigma' f'}{mF}\right)\right]$$

and since the quantity in the square brackets is a constant with respect to the w integration we can immediately write

$$\frac{mF}{qE}\left(1 + \int_0^\infty dw' \frac{n_A\sigma' f'}{mF}\right) = \frac{mF}{p}\left\{\int_\varepsilon^\infty dw\, e^{-\int_\varepsilon^w \frac{1}{qE}(p + n_A\sigma')dw'}\right\}^{-1} \tag{A4}$$

Using this result in equation (A3) we find the final form for the distribution function, namely

$$\bar{f}(w) = \frac{mF}{p} H(w - \varepsilon) \frac{e^{-\int_0^w \frac{1}{qE}(p + n_A\sigma')dw'}}{\int_\varepsilon^\infty dw\, e^{-\int_\varepsilon^w \frac{1}{qE}(p + n_A\sigma')dw'}} \tag{A6}$$

Letting $\varepsilon \to 0$, we see that we obtain equation (7). Notice that the small factor ε has been used to avoid any problems at $w = 0$. As was mentioned earlier, we assumed that $\bar{f}(w=0) = 0$, and we will now show that this is the case. Integrating equation (A1) from $w = 0$ to $w = \infty$ and canceling like terms we have

$$\bar{f}(w=\infty) - \bar{f}(w=o) + \frac{p}{qE}\int_0^\infty \bar{f}(w)dw = \frac{mF}{qE} \tag{A6}$$

Because a distribution function that increased as w goes to infinity is unphysical, we have the usual requirement that f go to zero as $w \to \infty$. Now using equation (A3) in (A6). along with the condition at $w = \infty$, we see that $\bar{f}(w=0) = 0$. Further details on the actual derivation

of equation (A1), as was mentioned in the text, can be found in reference (1).

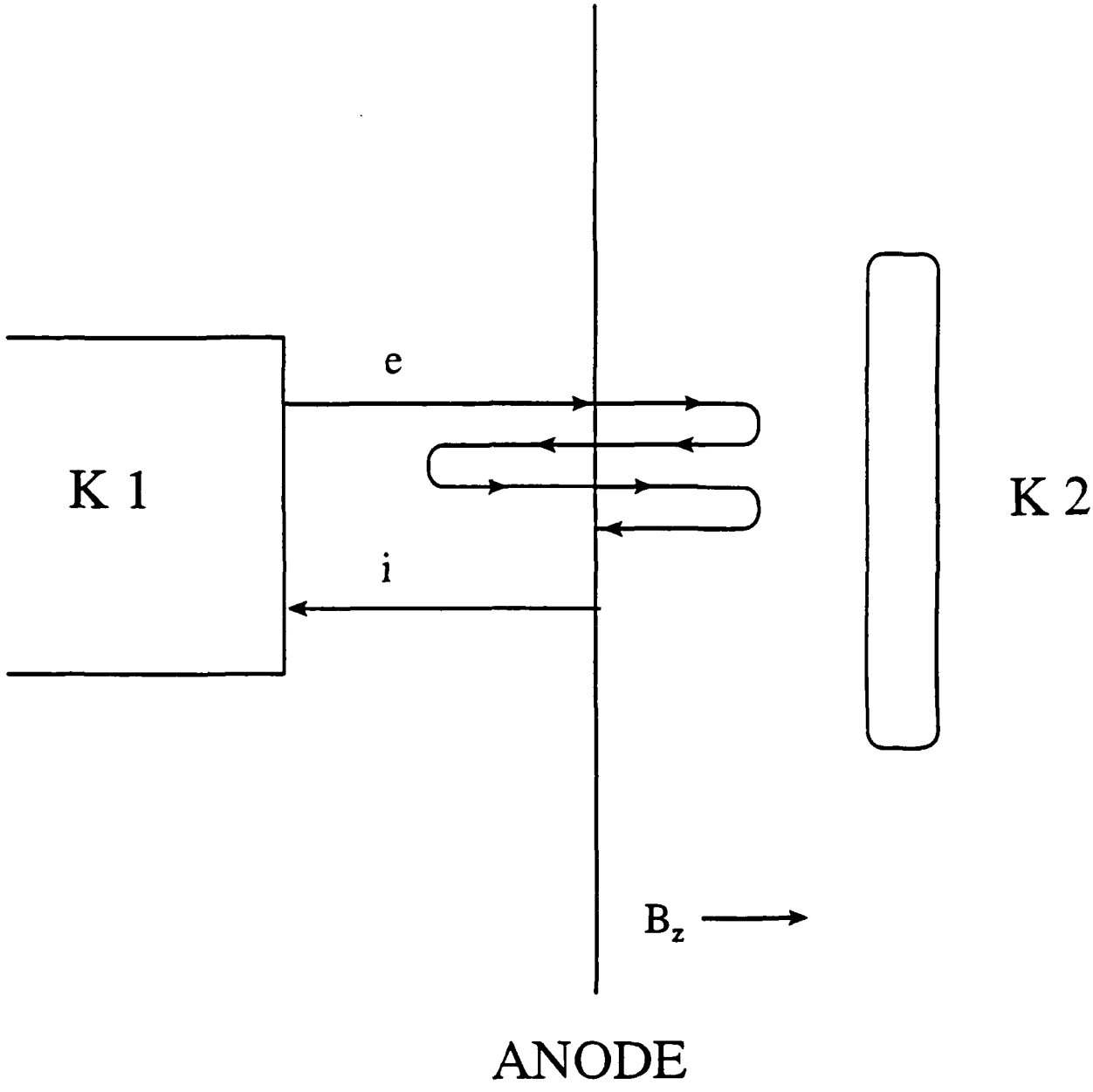

Figure 1. Closed Mode of the Reflex Switch.

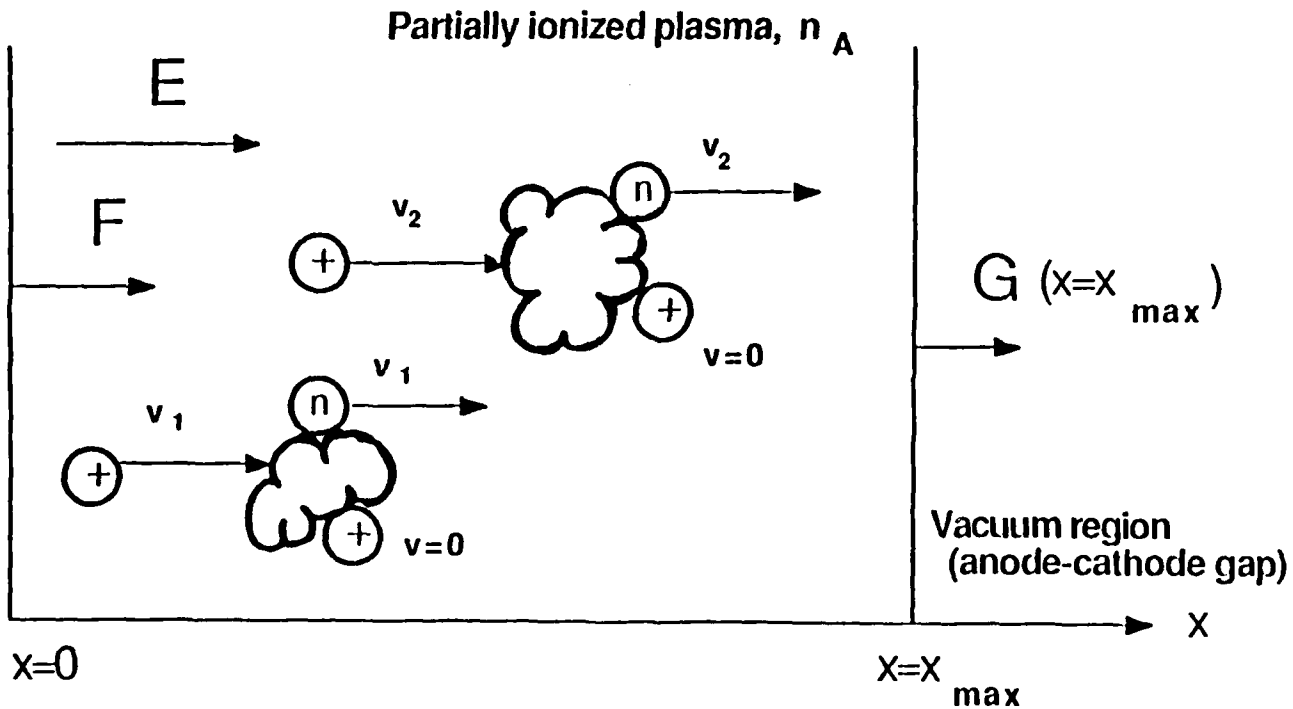

Charge Exchange Model

Figure 2

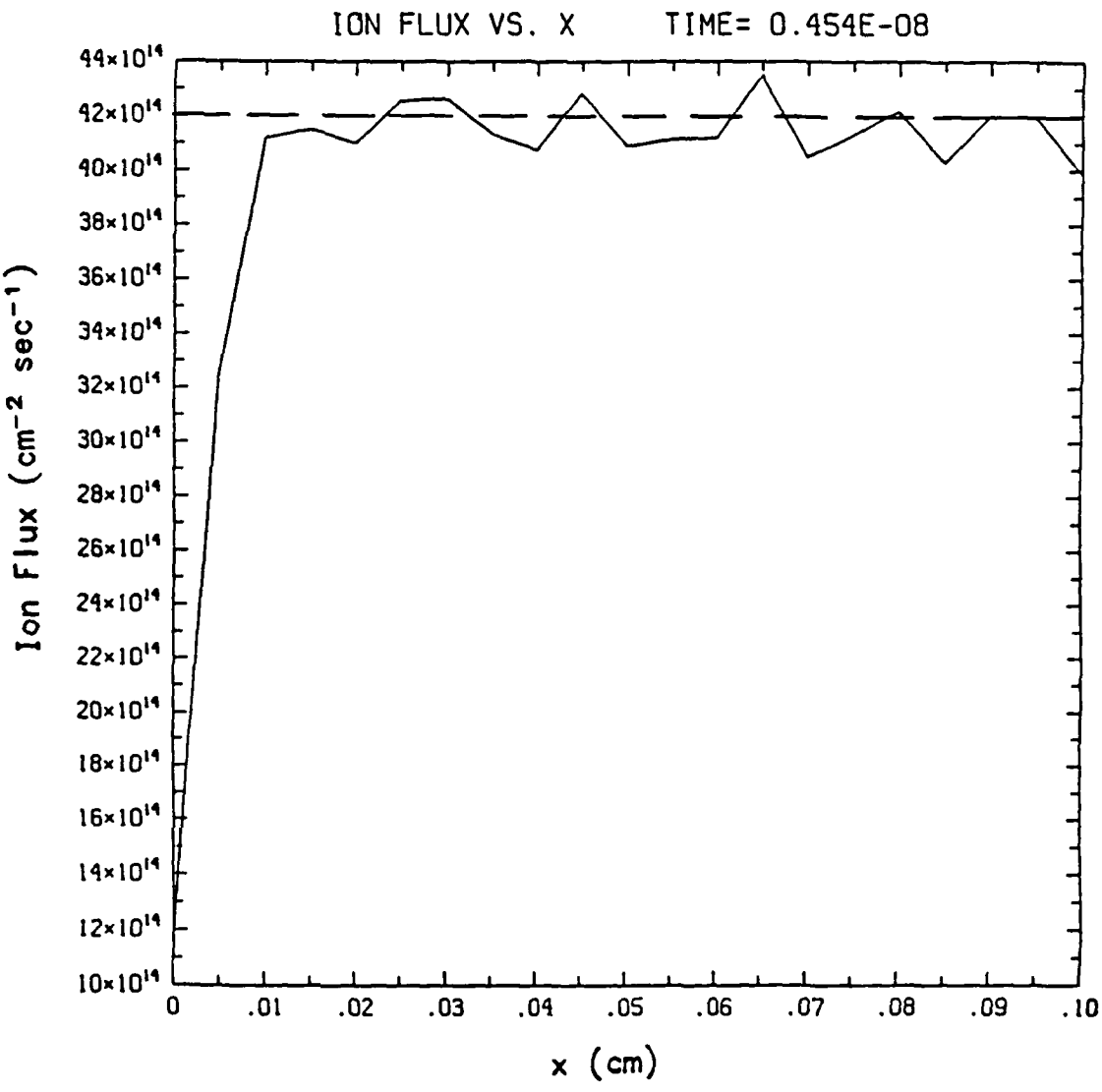

Ion Flux as a Function of x

Figure 3

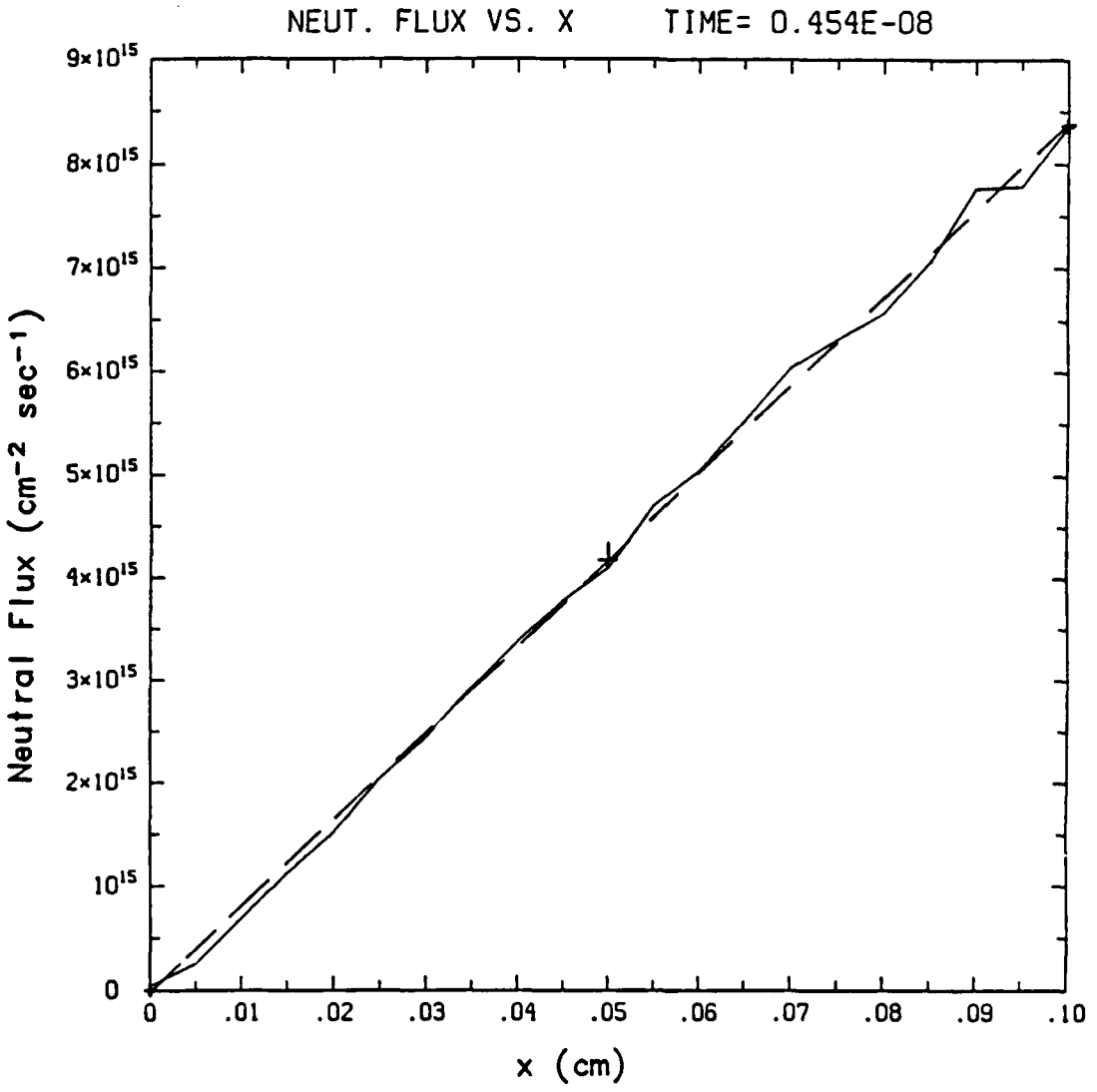

Neutral Flux as a Function of x

Figure 4

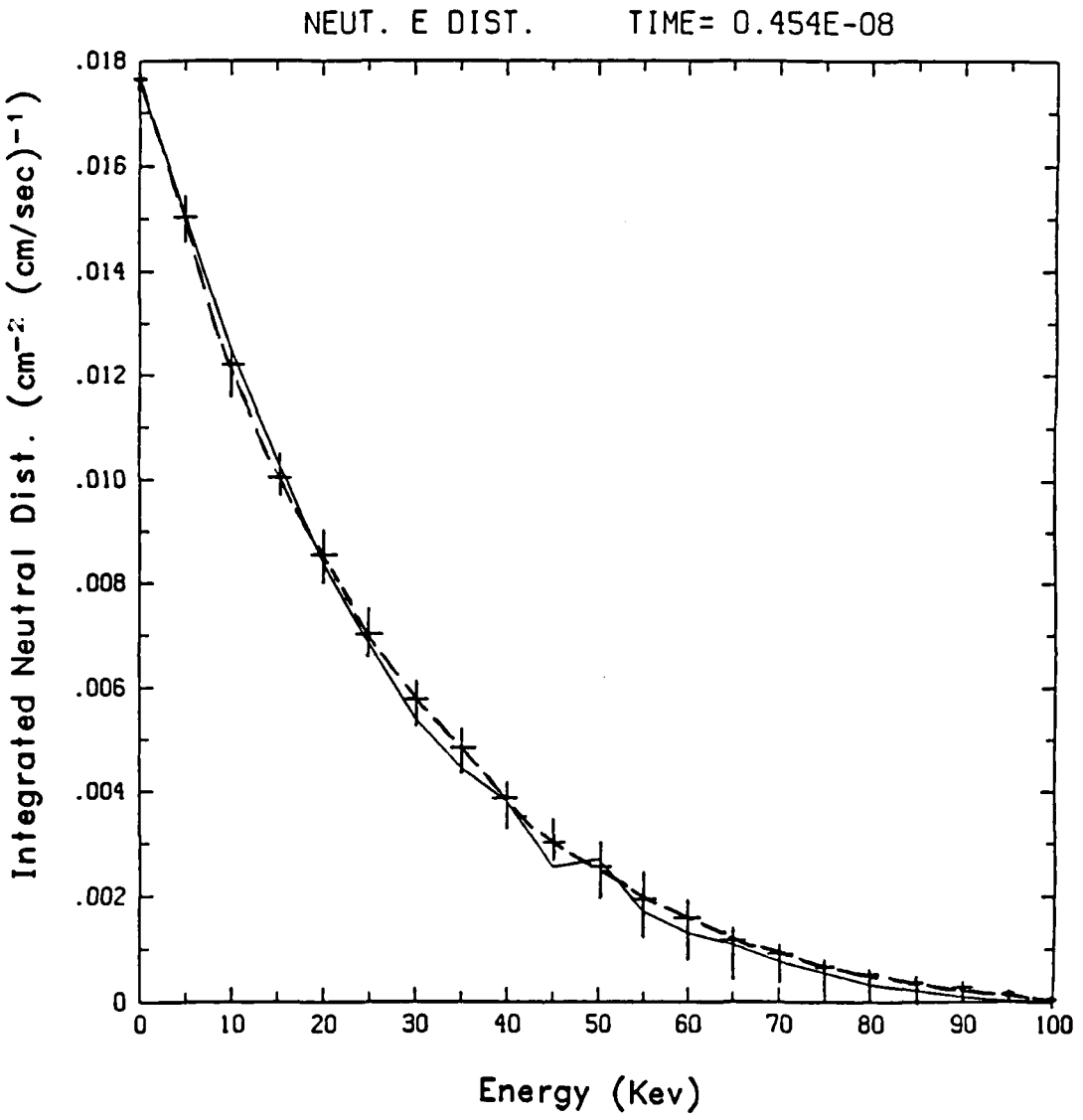

Integrated Neutral Distribution as a Function of Energy

Figure 5

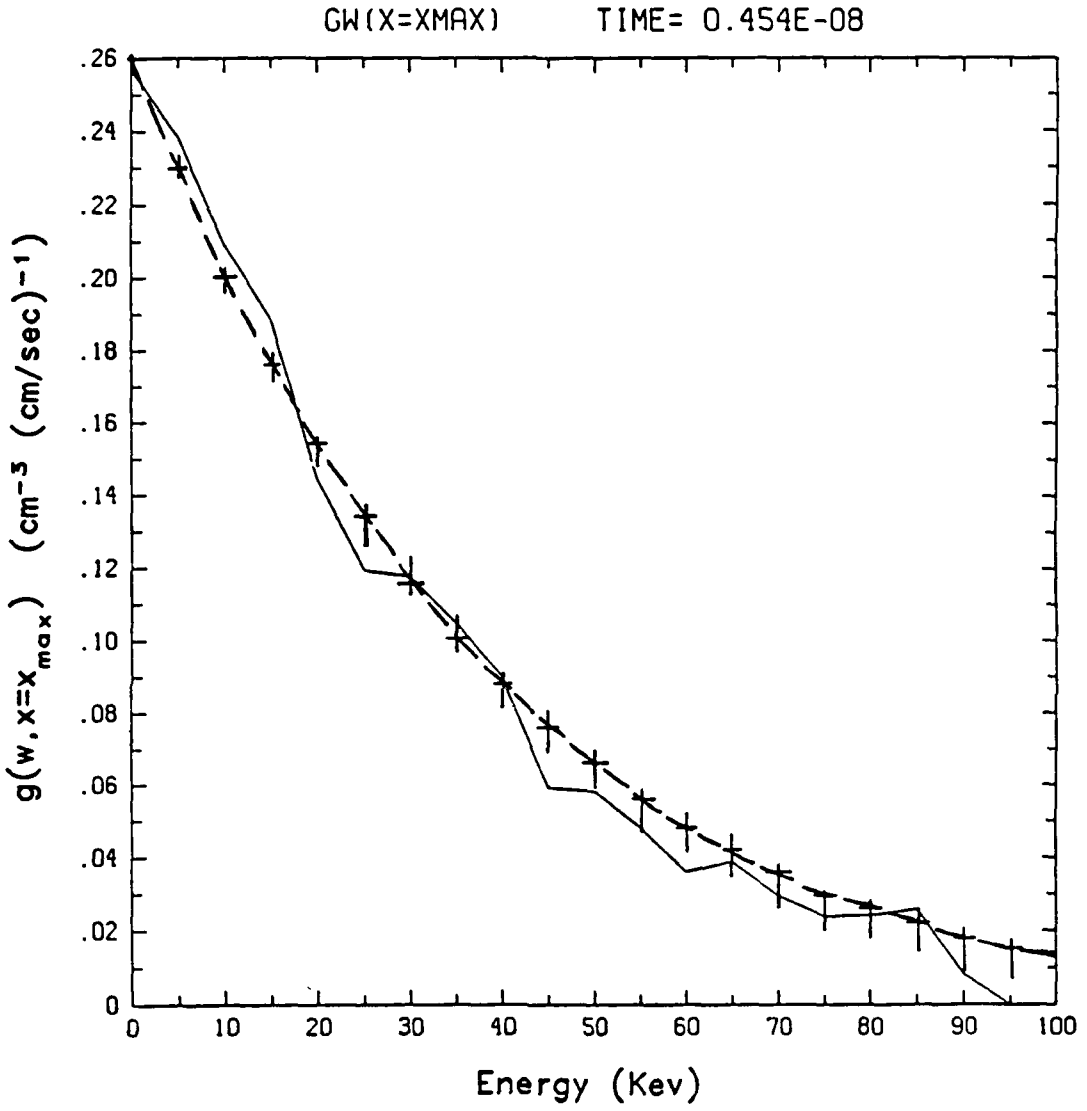

Neutral Distribution at the Vacuum Interface as a Function of Energy

Figure 6

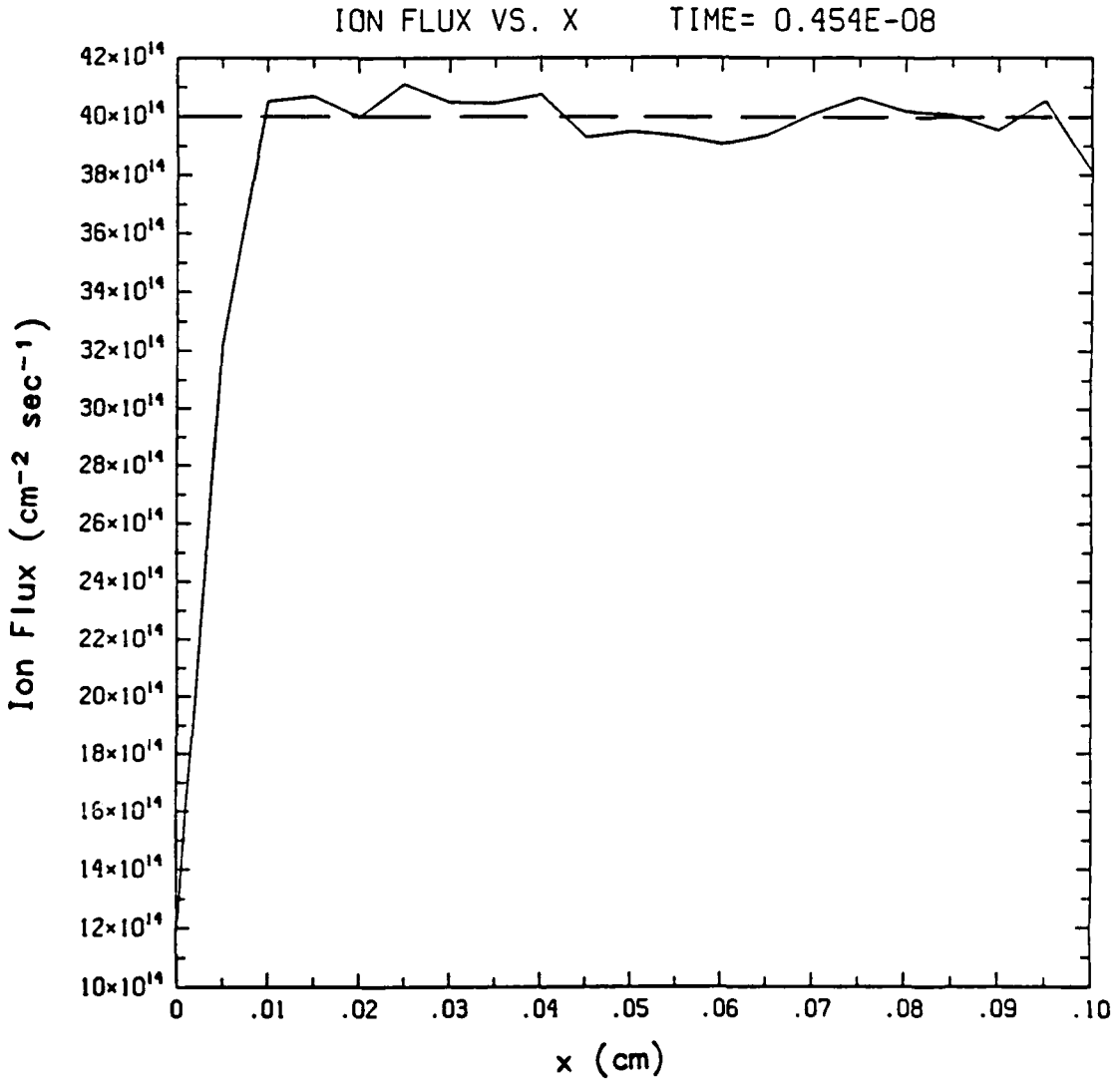

Ion Flux as a Function of x

Figure 7

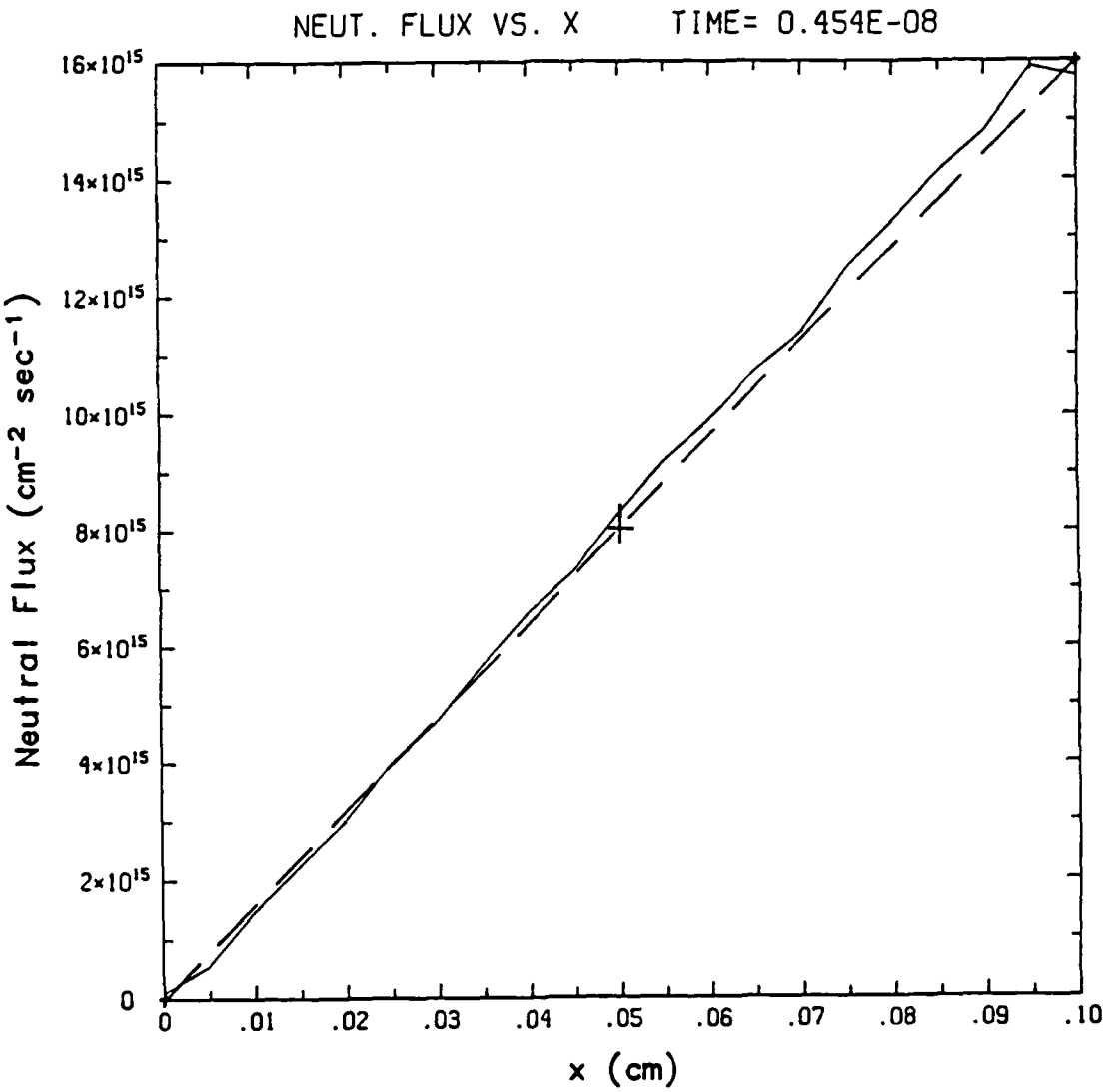

Neutral Flux as a Function of x

Figure 8

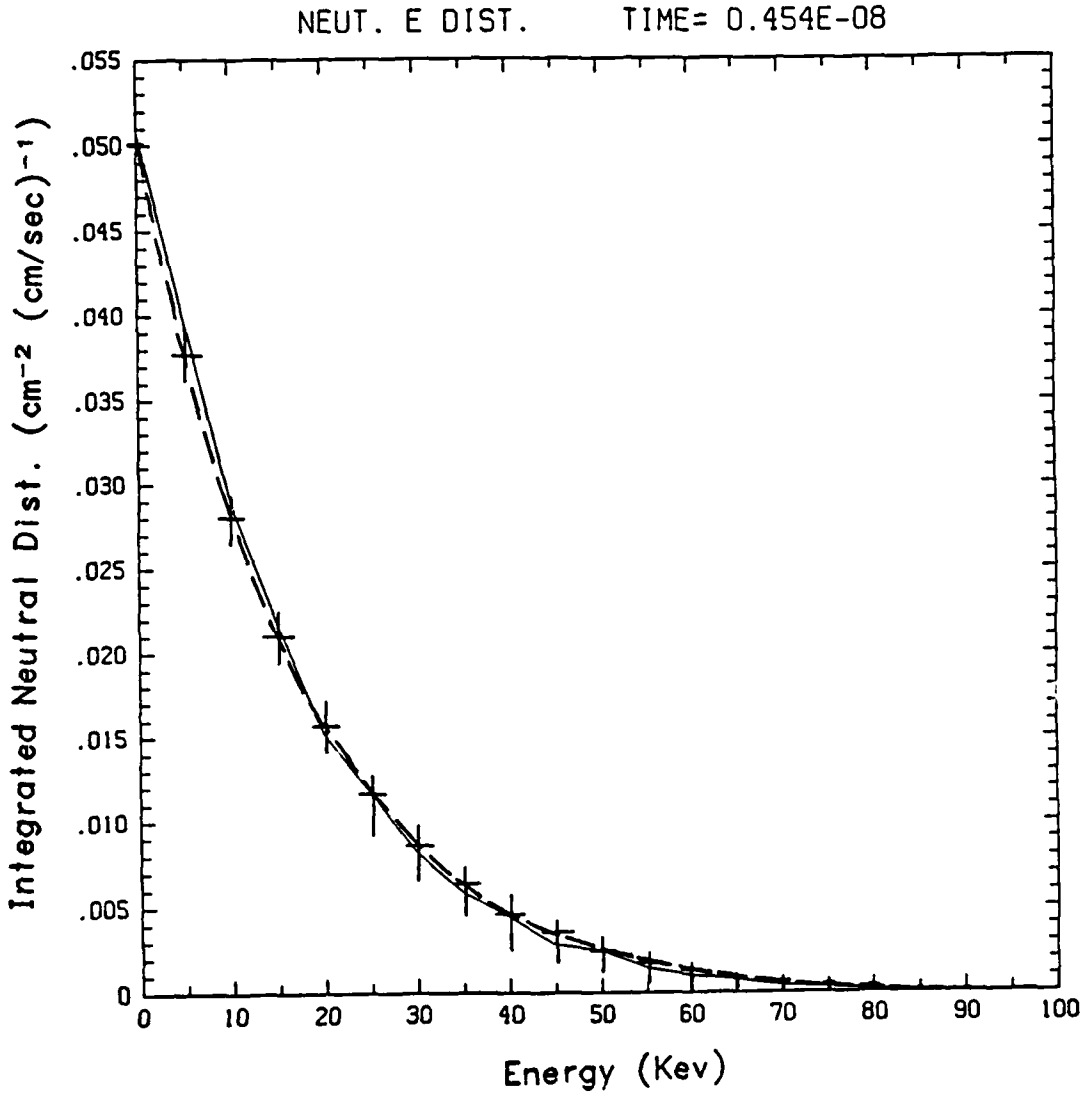

Integrated Neutral Distribution as a Function of Energy

Figure 9

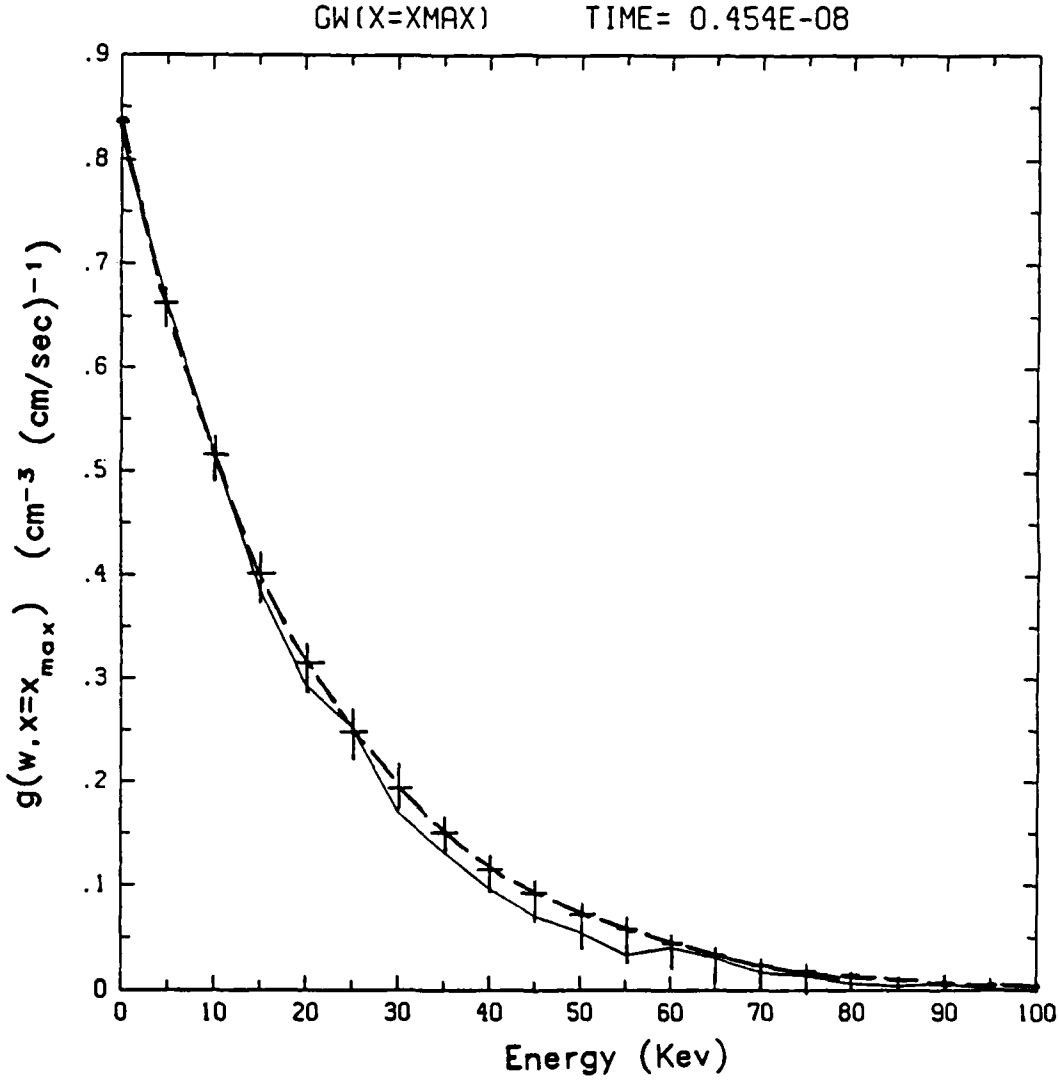

Neutral Distribution at the Vacuum Interface as a Function of Energy

Figure 10

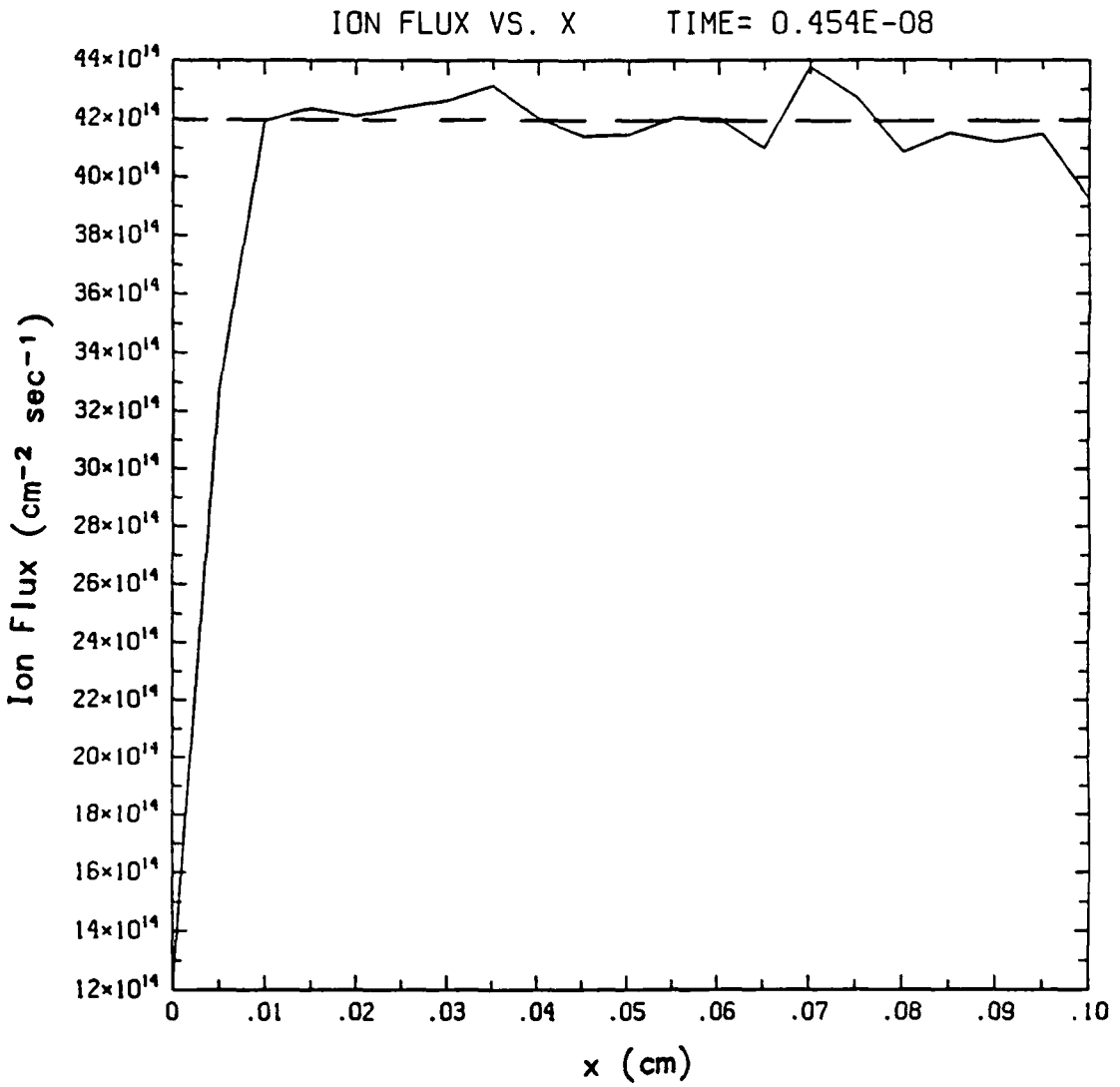

Ion Flux as a Function of x

Figure 11

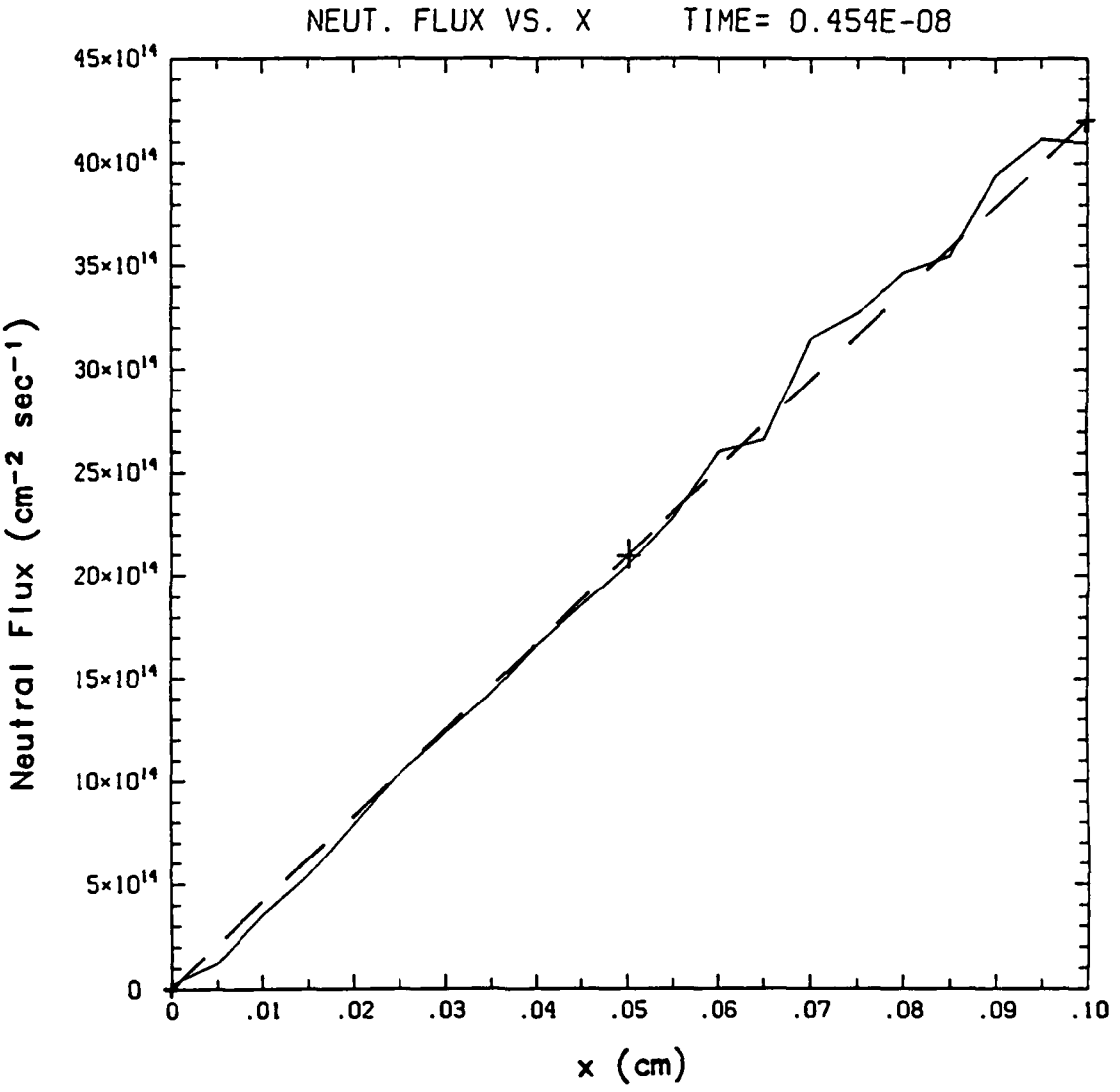

Neutral Flux as a Function of x

Figure 12

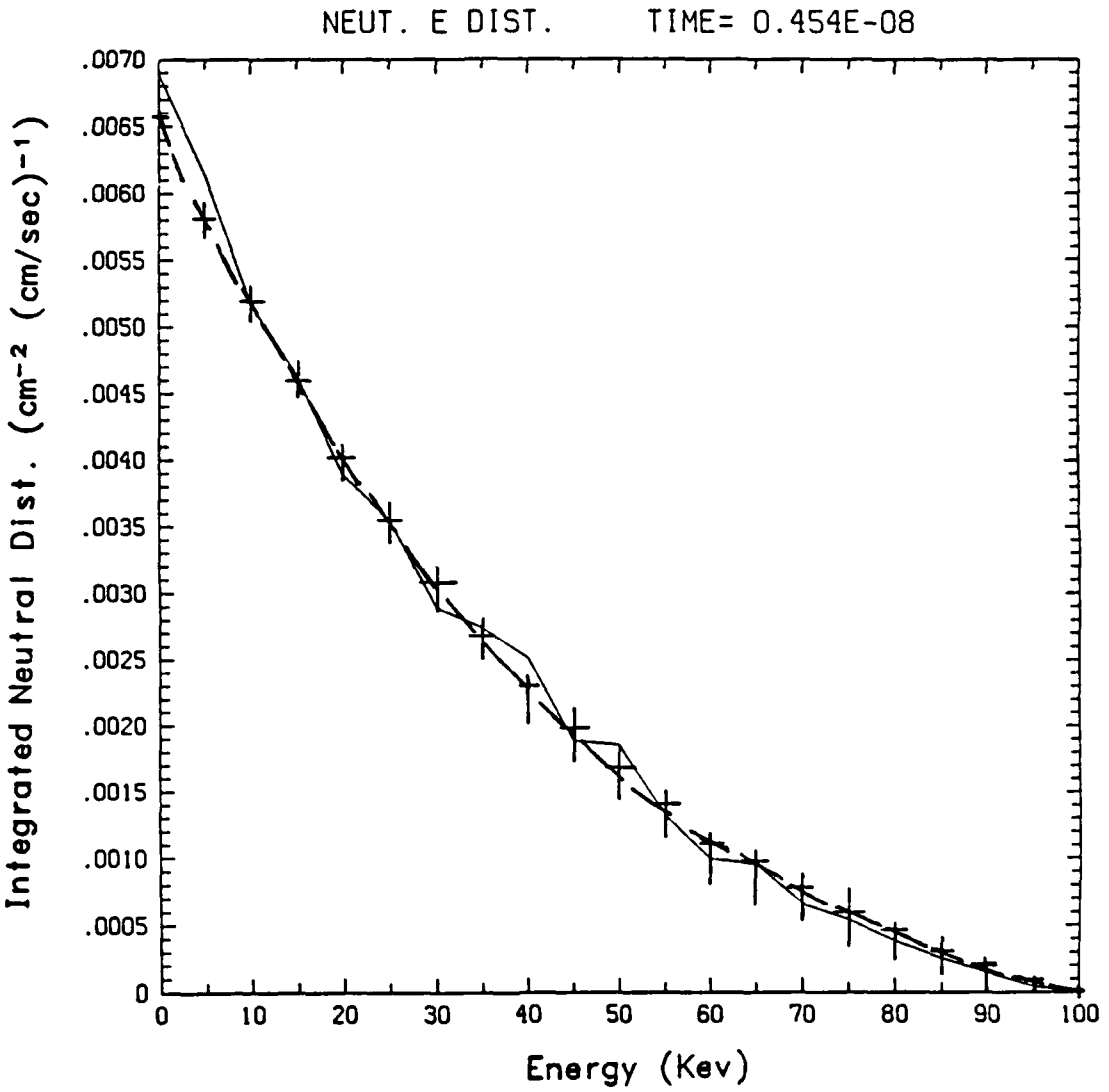

Integrated Neutral Distribution as a Function of Energy

Figure 13

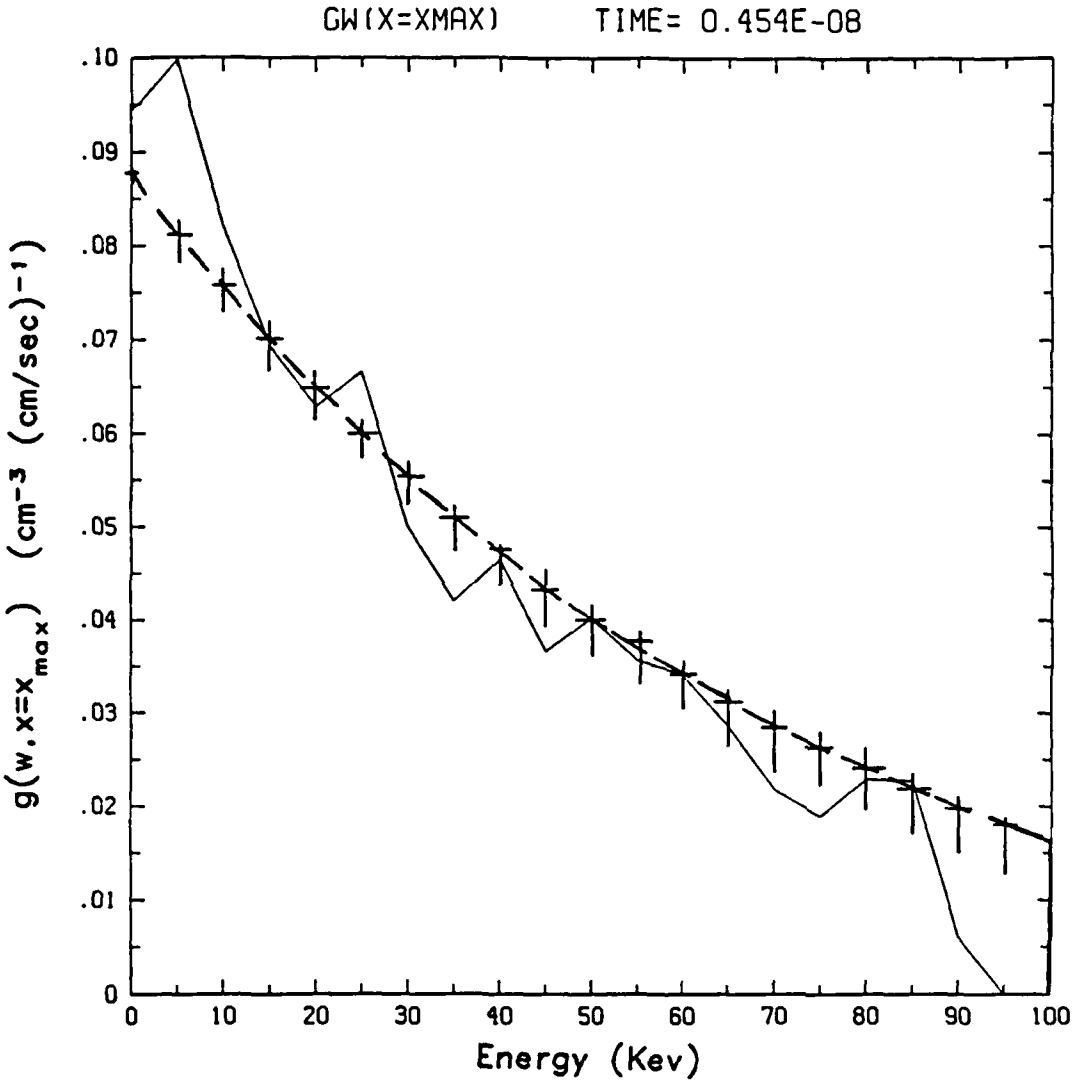

Neutral Distribution at the Vacuum Interface as a Function of Energy

Figure 14

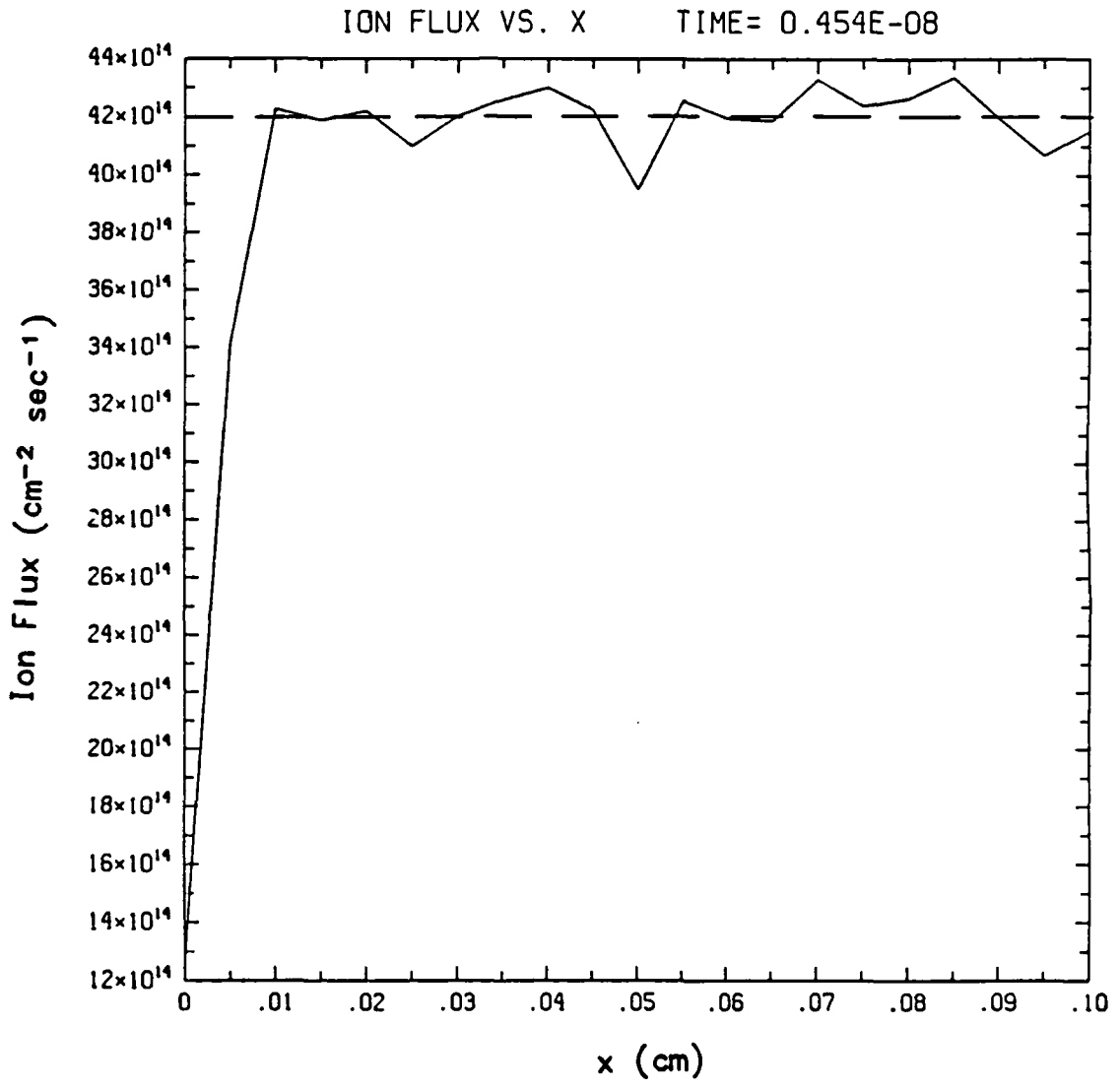

Ion Flux as a Function of x

Figure 15

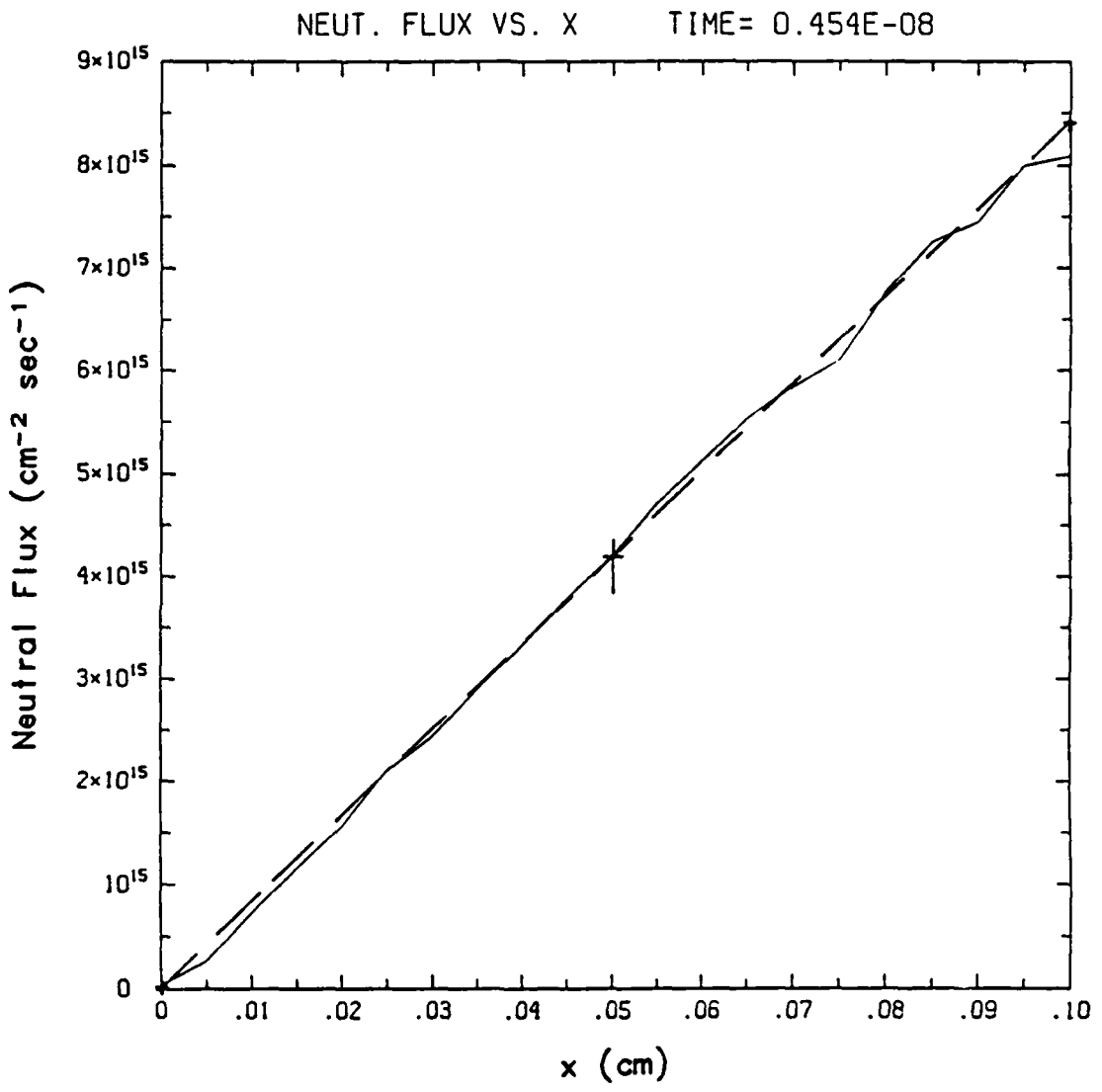

Neutral Flux as a Function of x

Figure 16

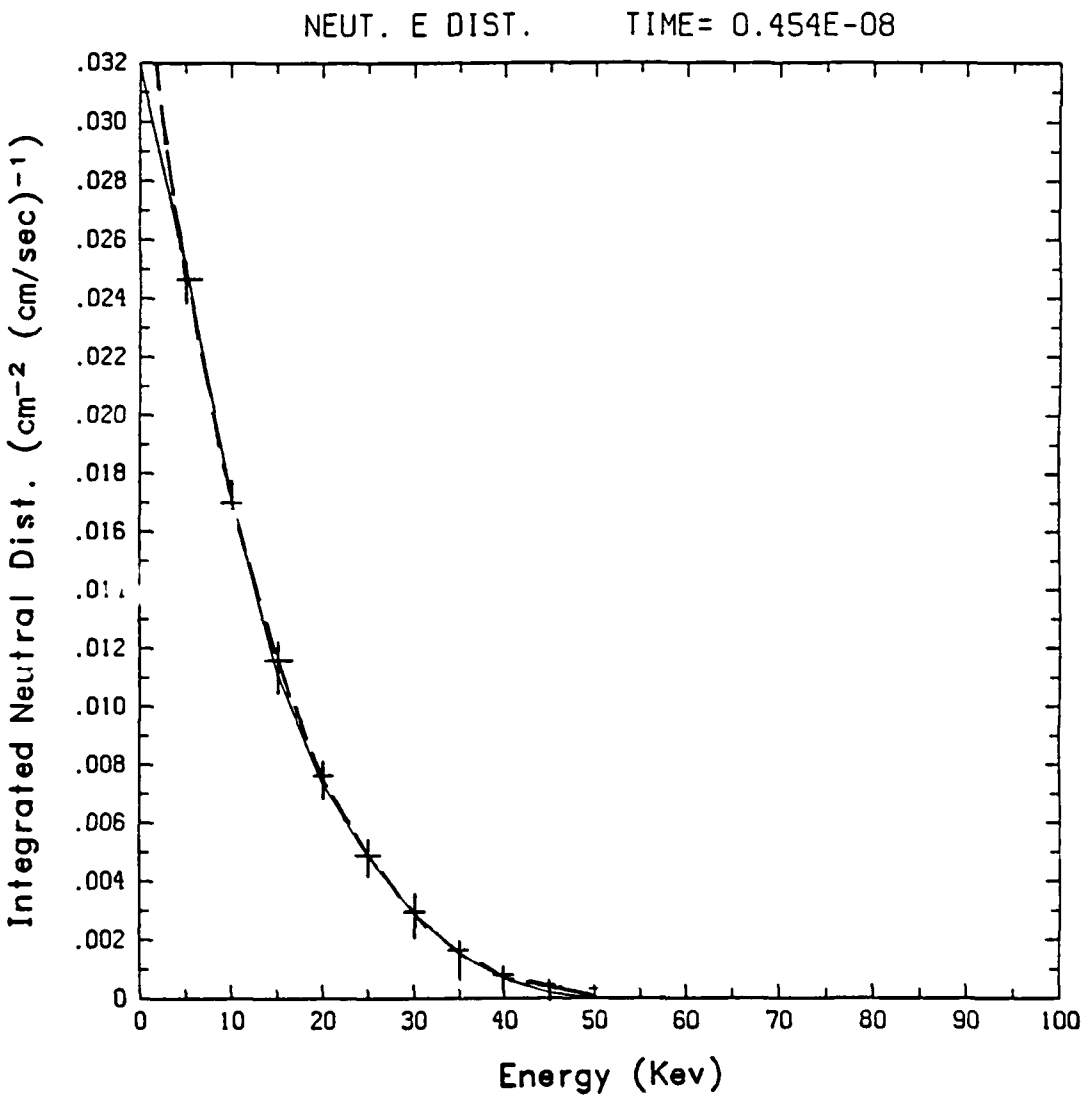

Integrated Neutral Distribution as a Function of Energy

Figure 17

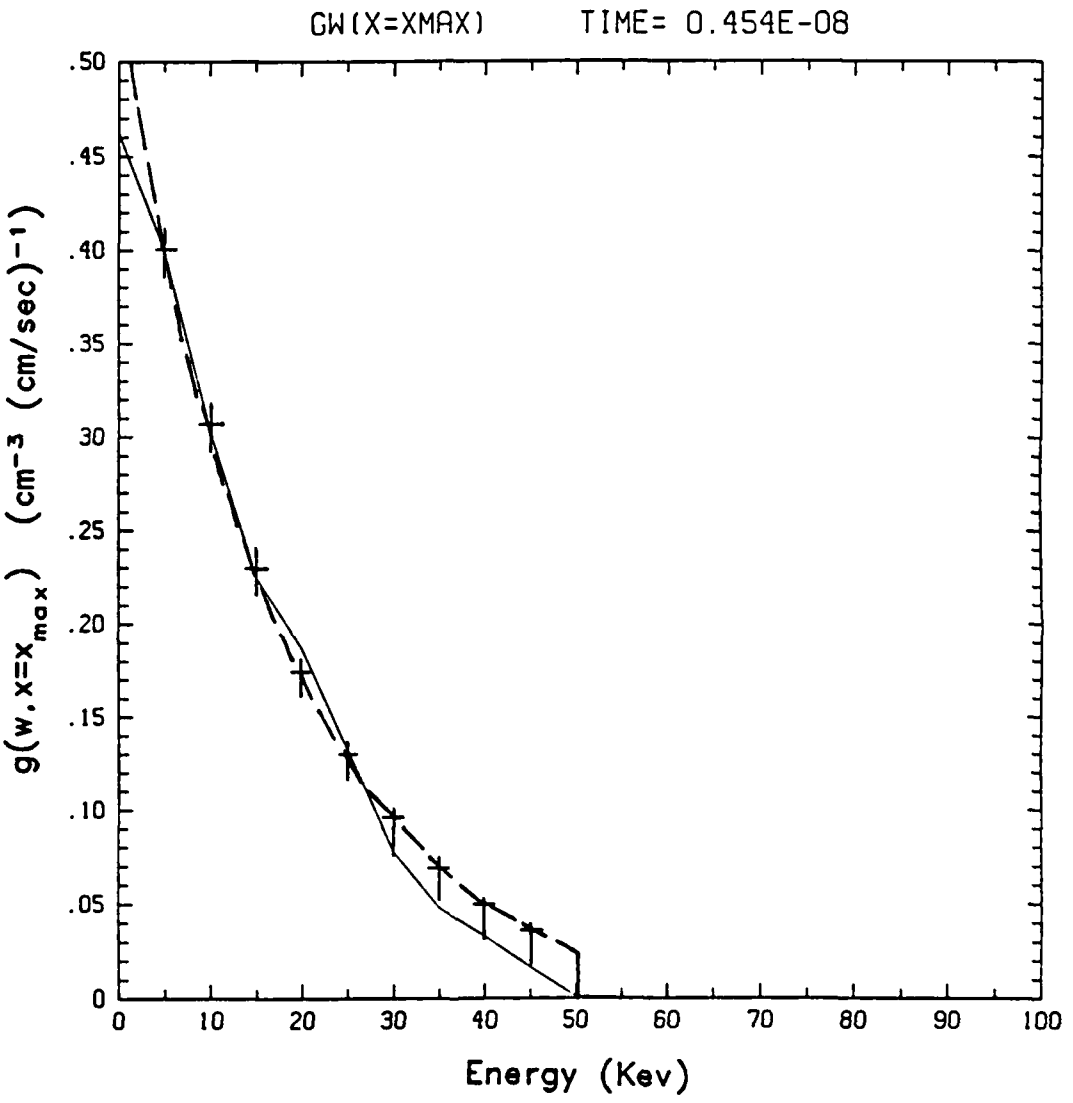

Neutral Distribution at the Vacuum Interface as a Function of Energy

Figure 18

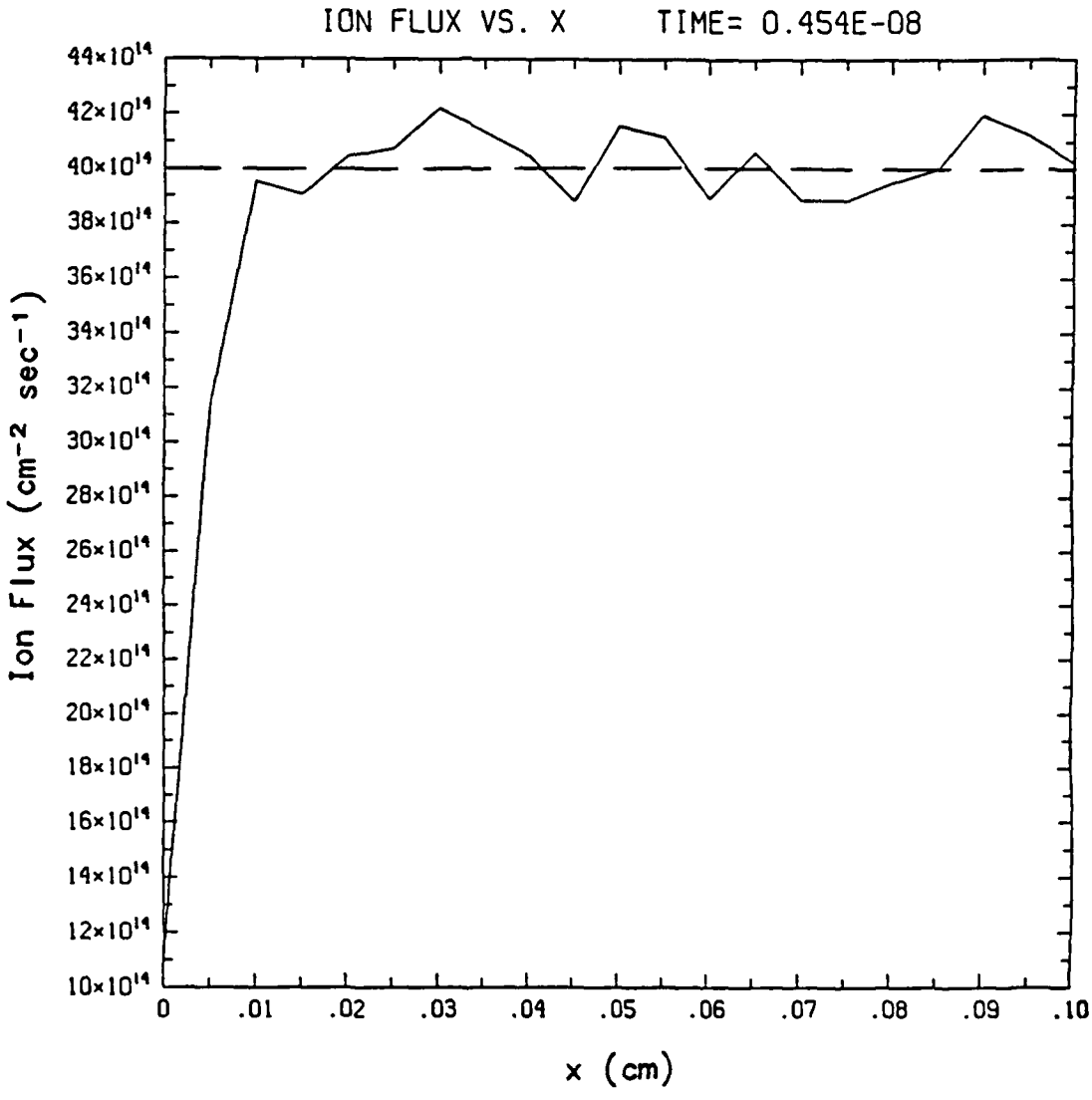

Neutral Flux as a Function of x

Figure 19

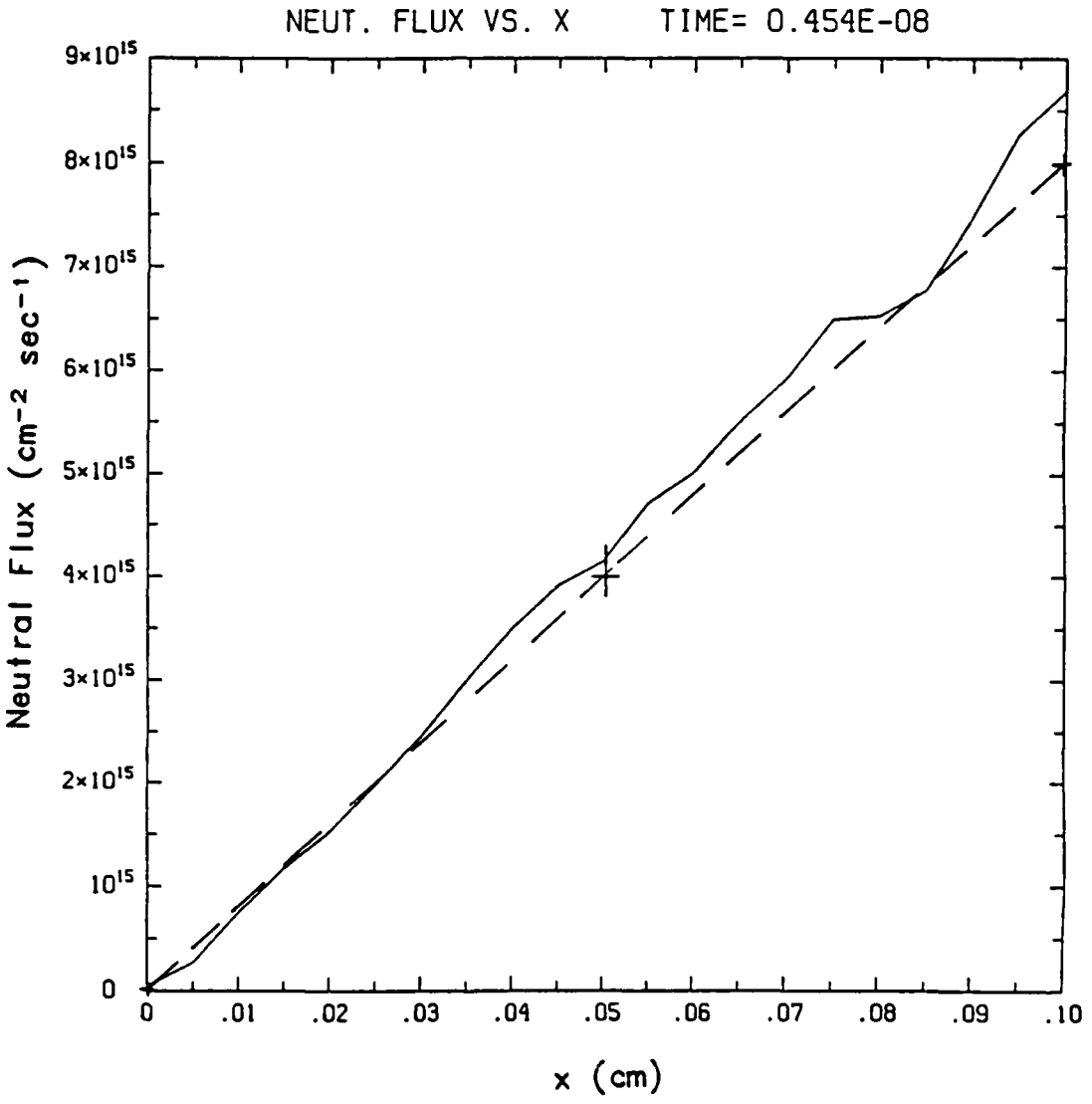

Neutral Flux as a Function of x

Figure 20

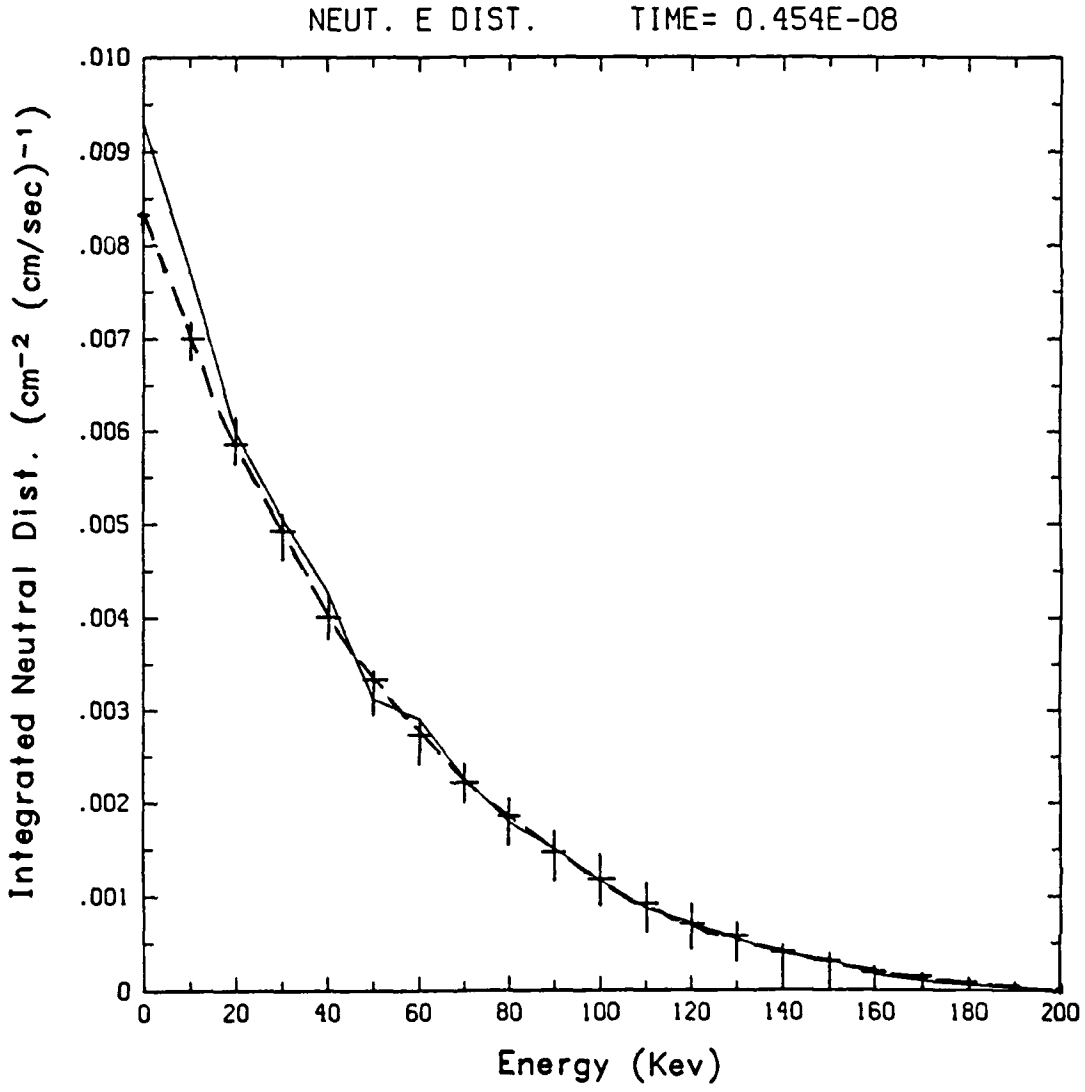

Integrated Neutral Distribution as a Function of Energy

Figure 21

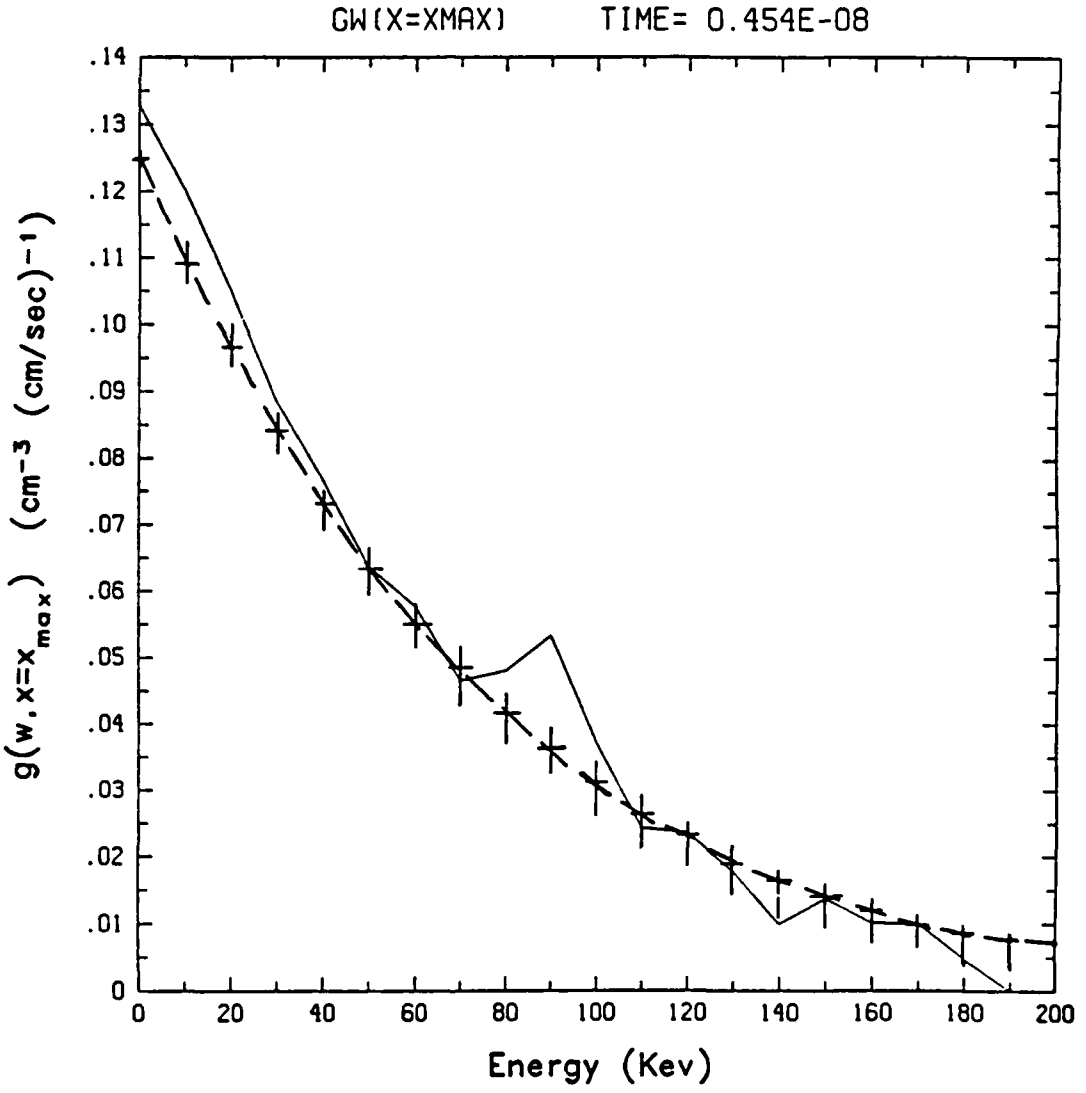

Neutral Distribtuion at the Vacuum Interface as a Function of Energy

Figure 22

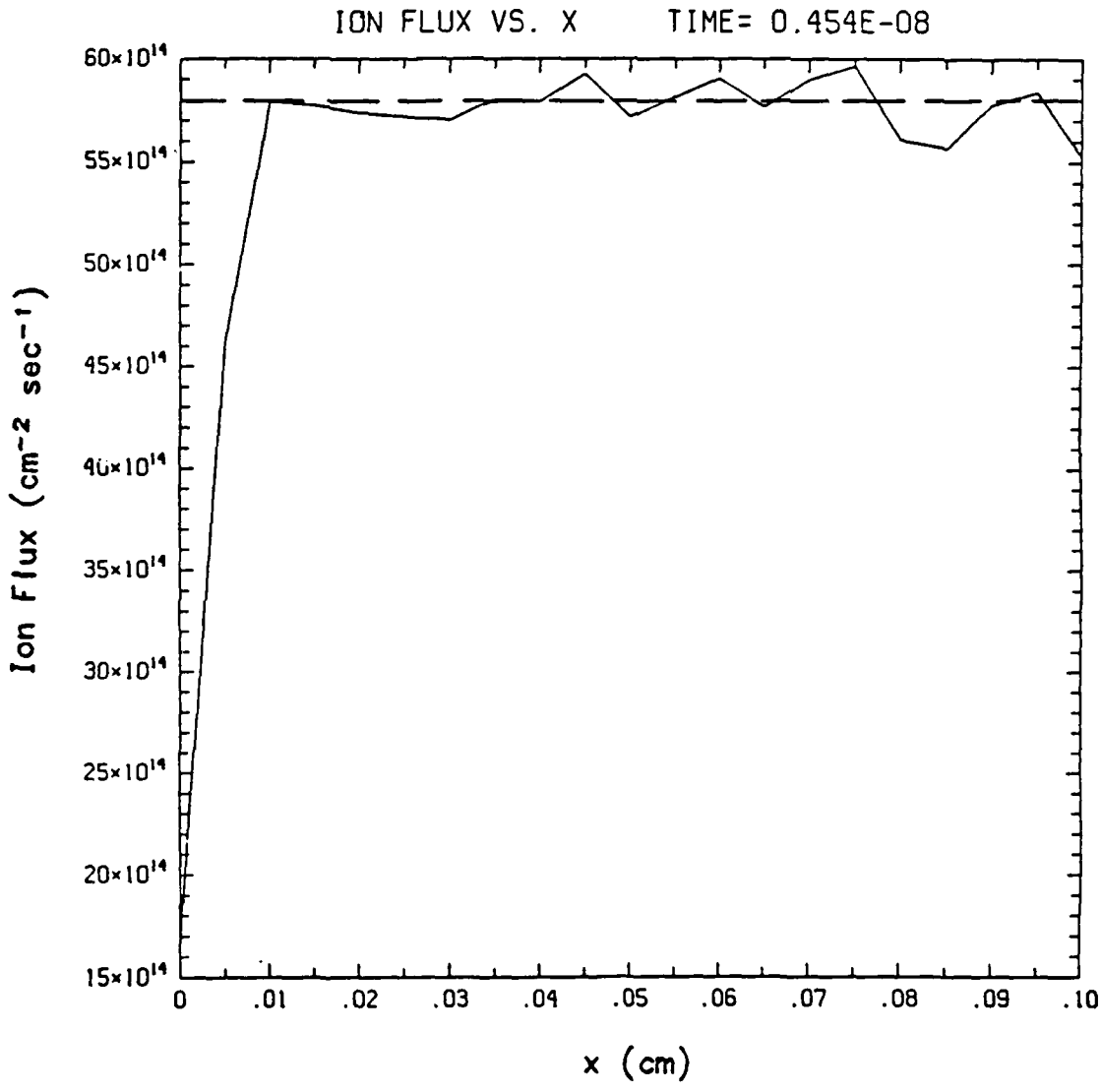

Ion Flux as a Function of x

Figure 23

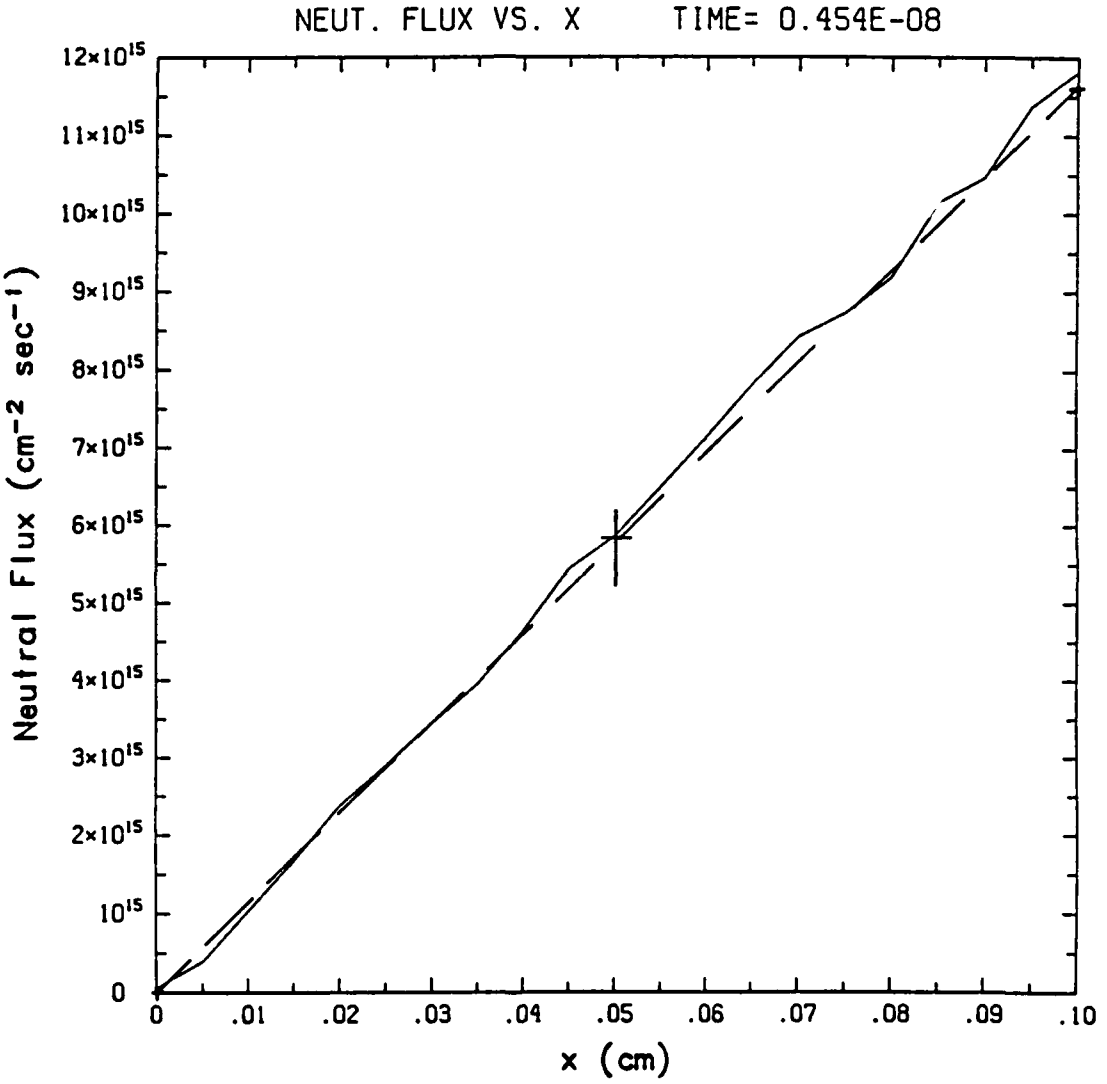

Neutral Flux as a Function of x

Figure 24

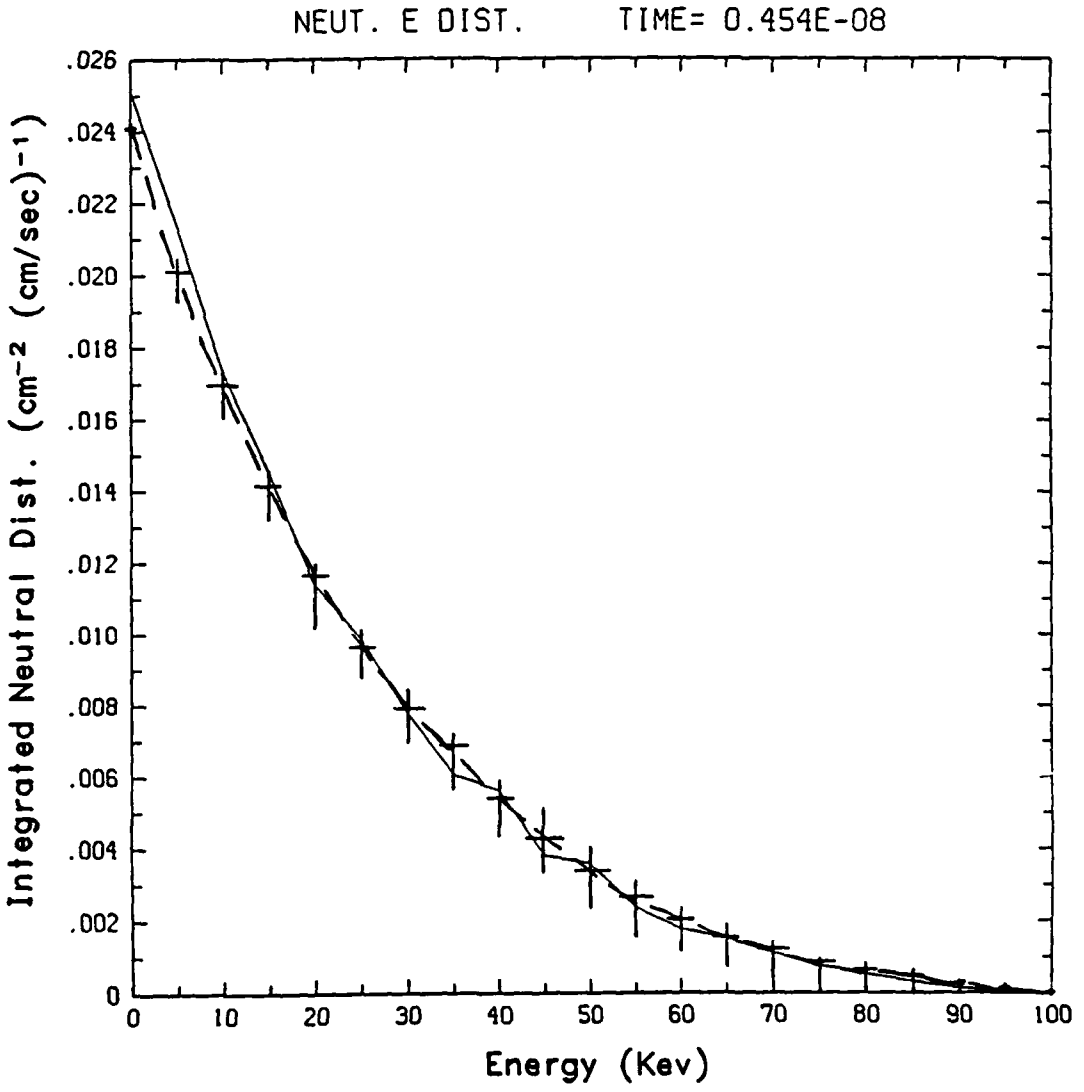

Integrated Neutral Distribution as a Function of Energy

Figure 25

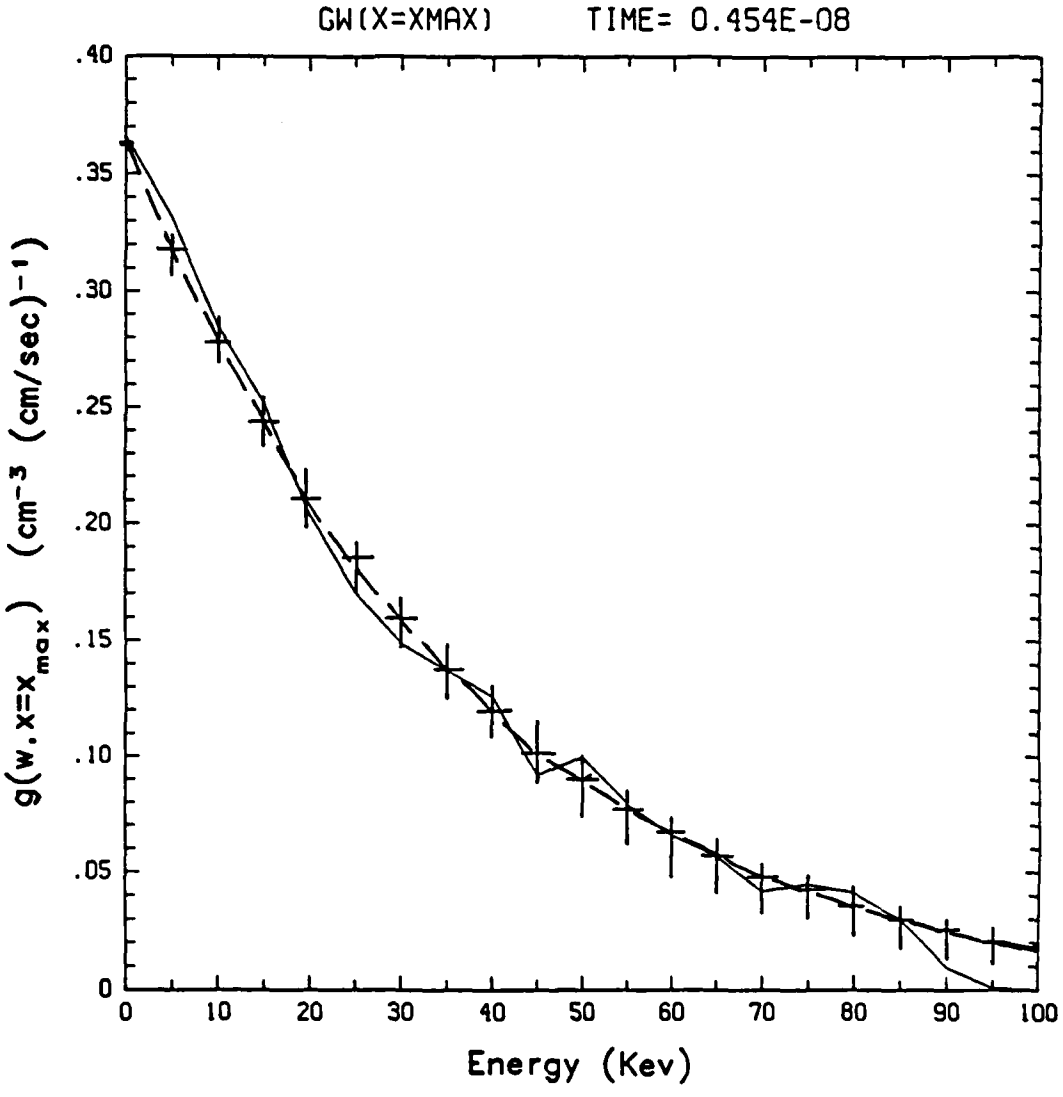

Neutral Distribution at the Vacuum Interface as a Function of Energy

Figure 26

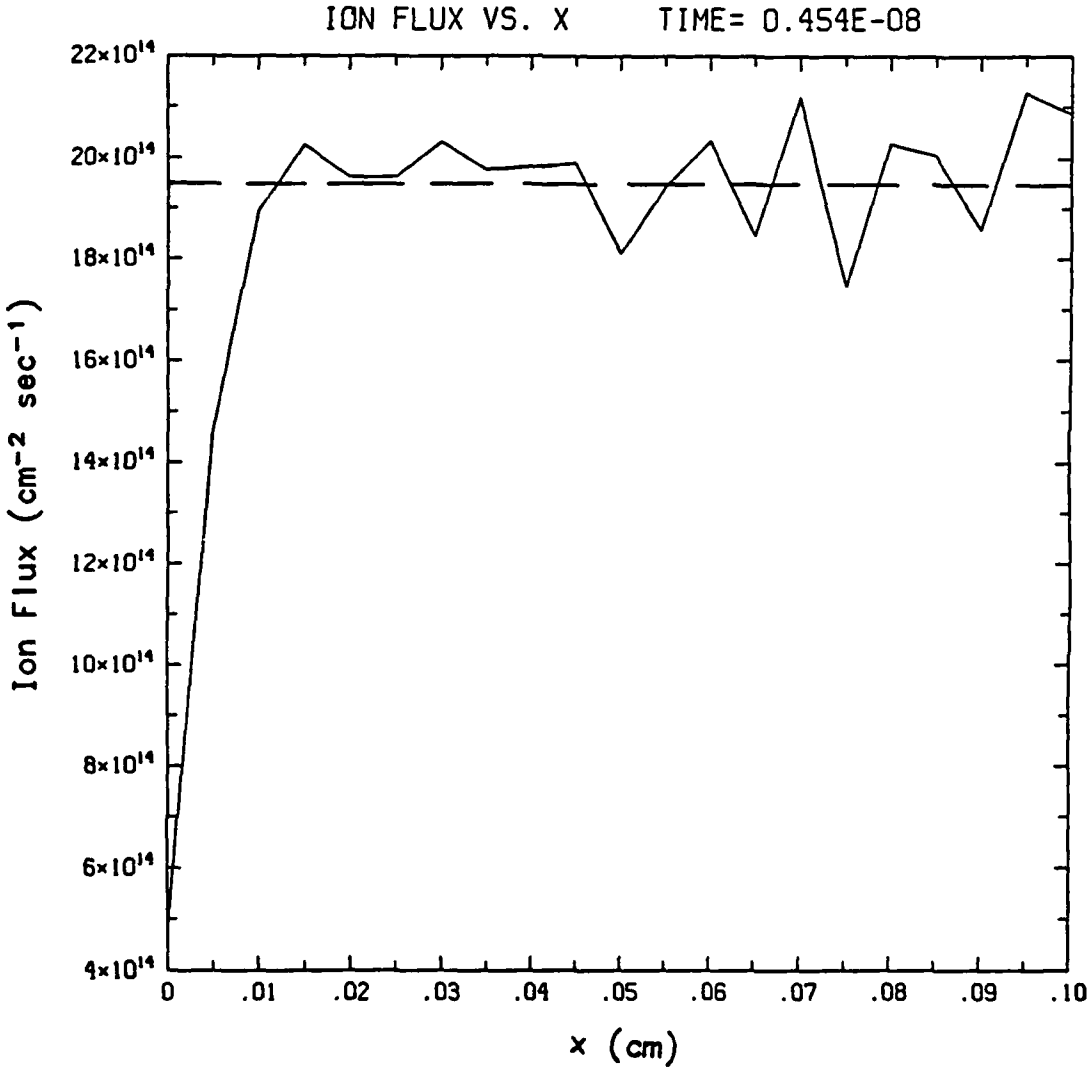

Ion Flux as a Function of x

Figure 27

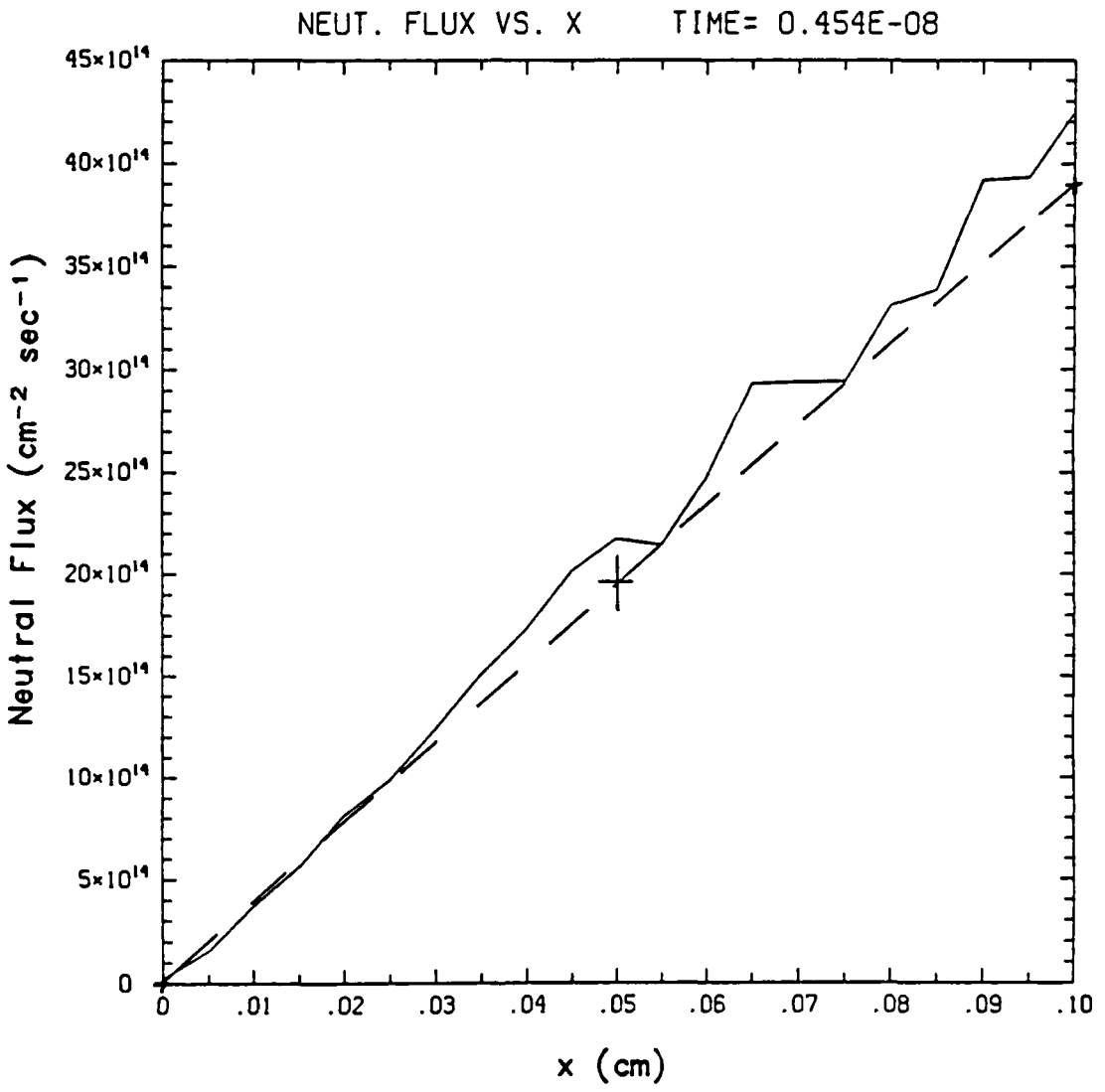

Neutral Flux as a Function of x

Figure 28

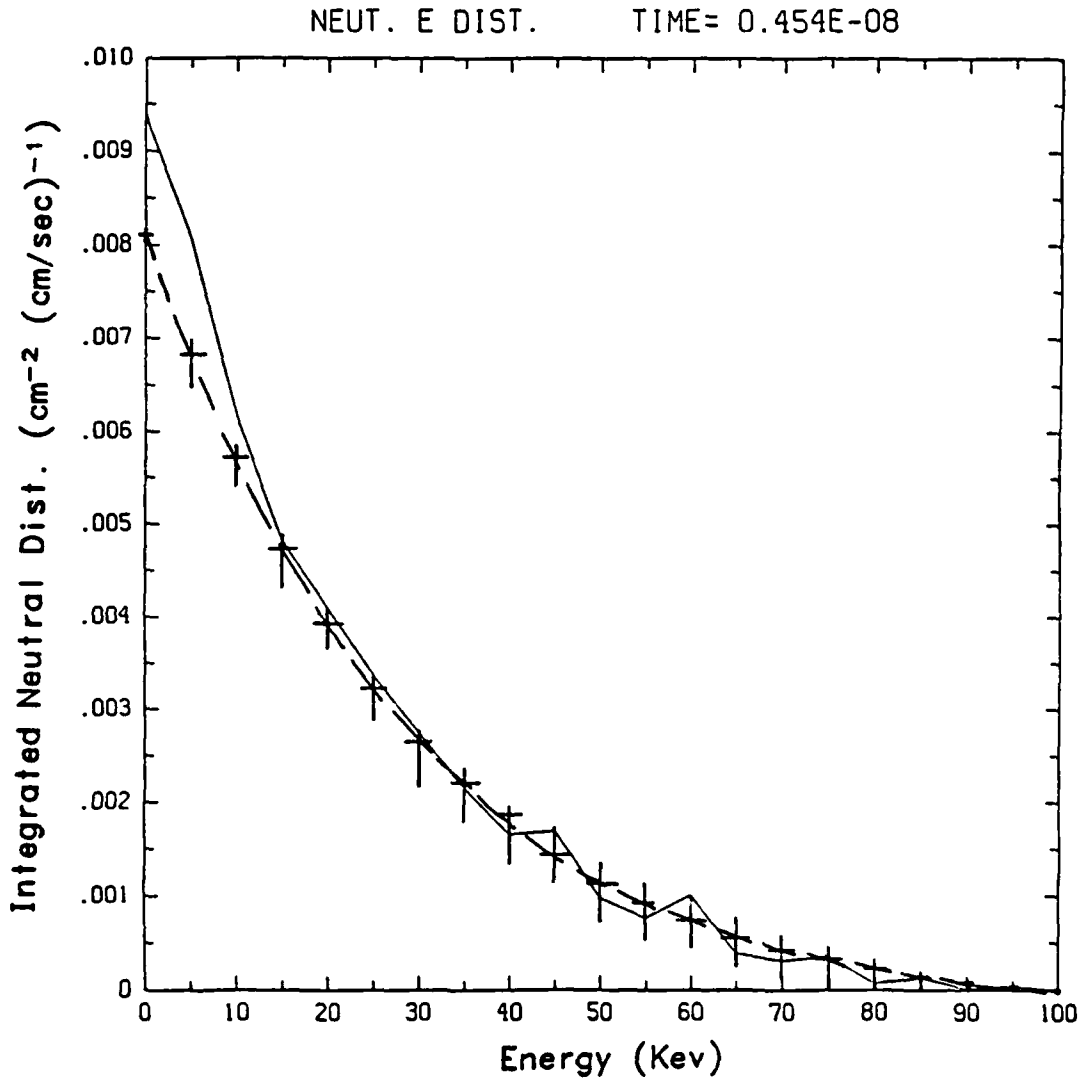

Integrated Neutral Distribution as a Function of Energy

Figure 29

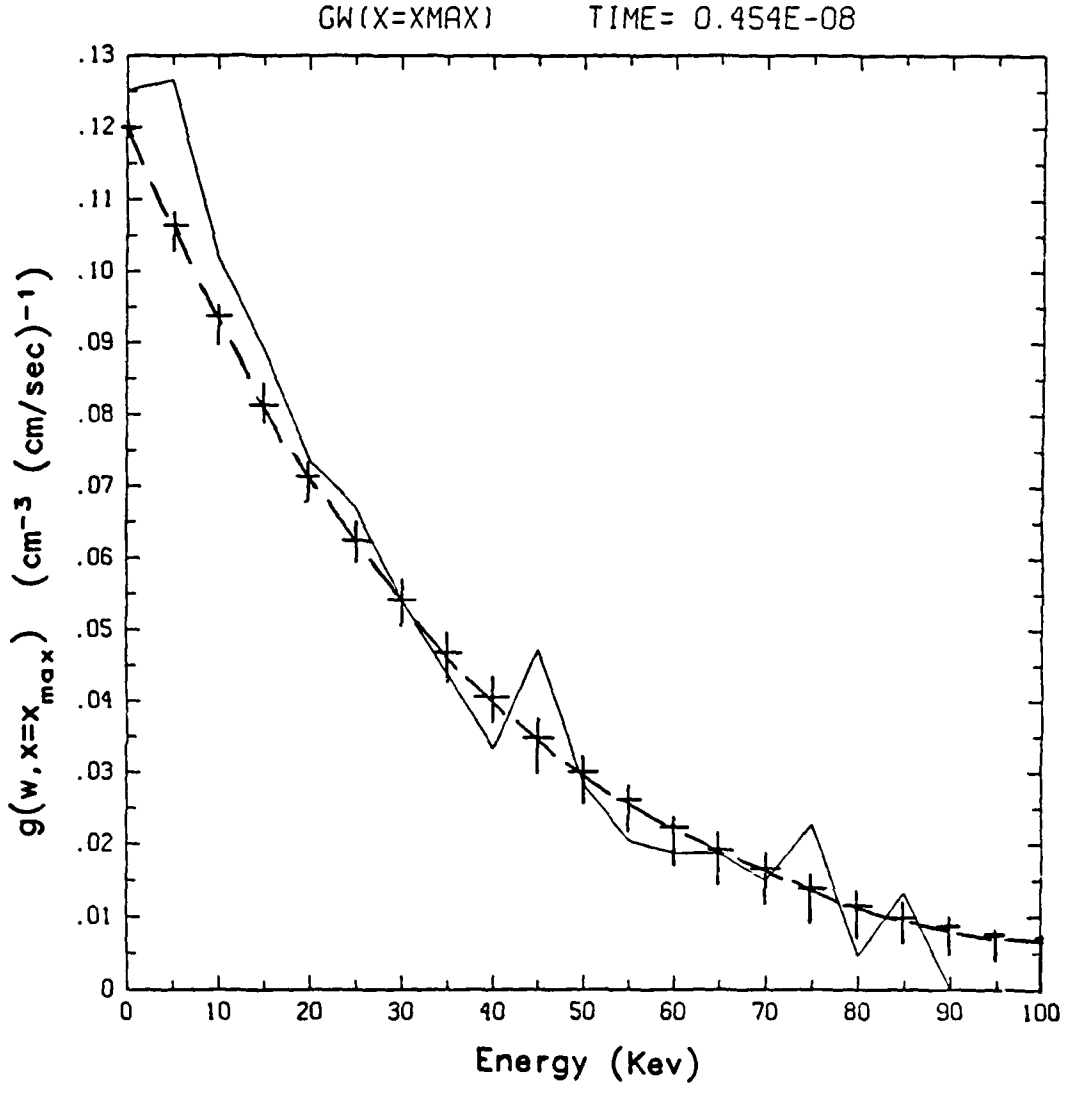

Neutral Distribution at the Vacuum Interface as a Function of Energy

Figure 30

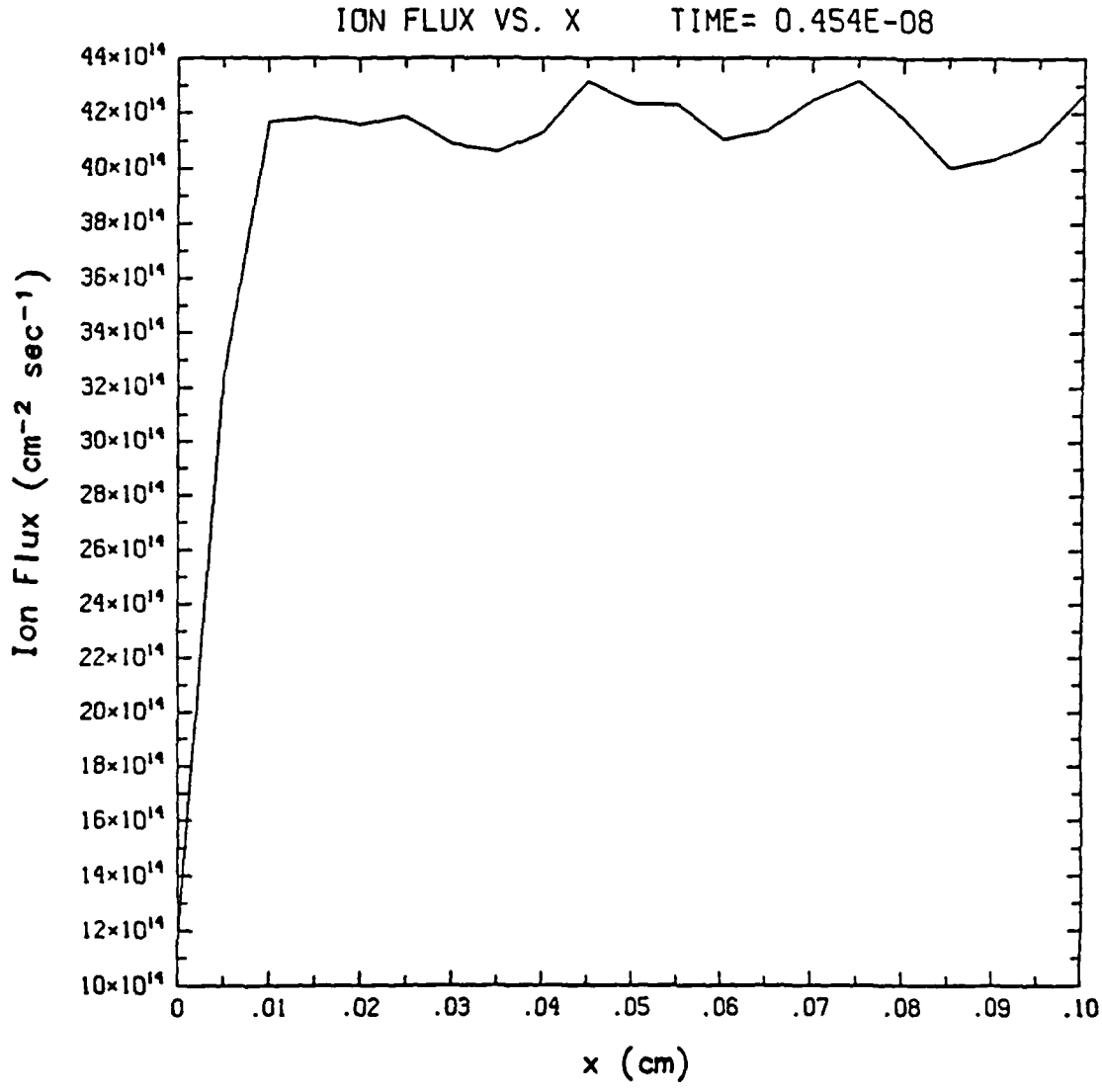

Ion Flux as a Function of x

Figure 31

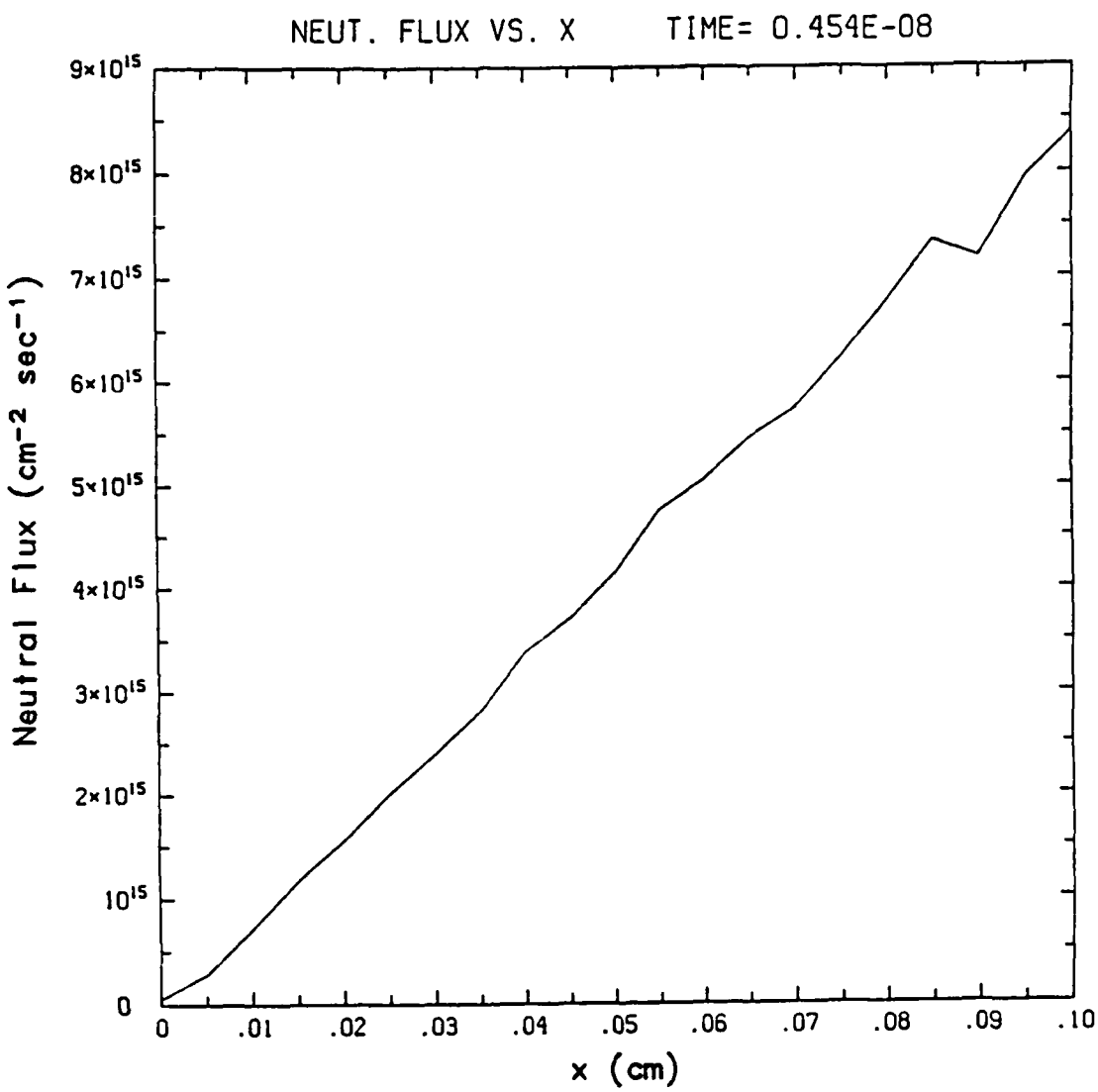

Neutral Flux as a Function of x

Figure 32

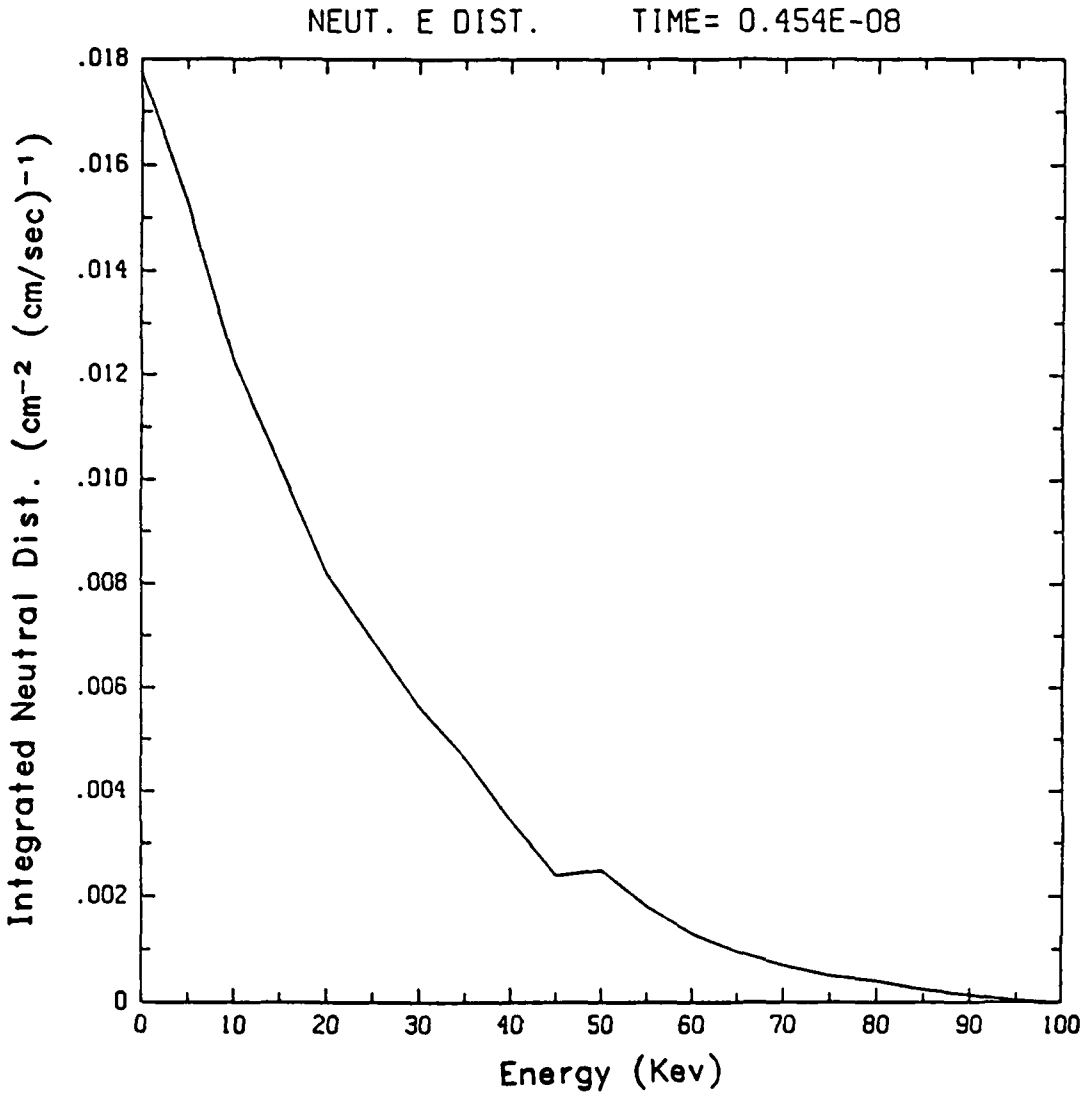

Integrated Neutral Distribution as a Function of Energy

Figure 33

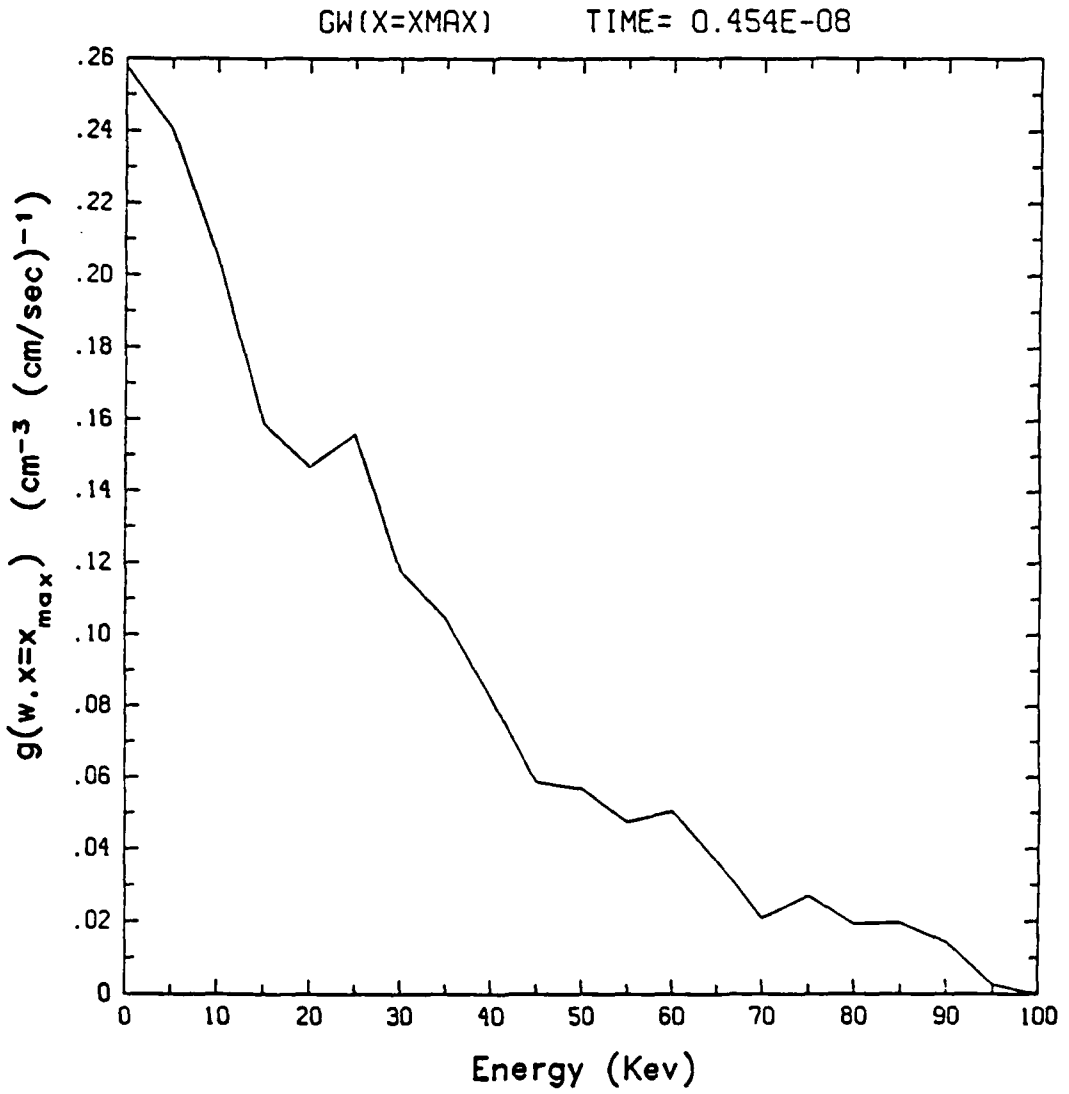

Neutral Distribution at the Vacuum Interface as a Function of Energy

Figure 34

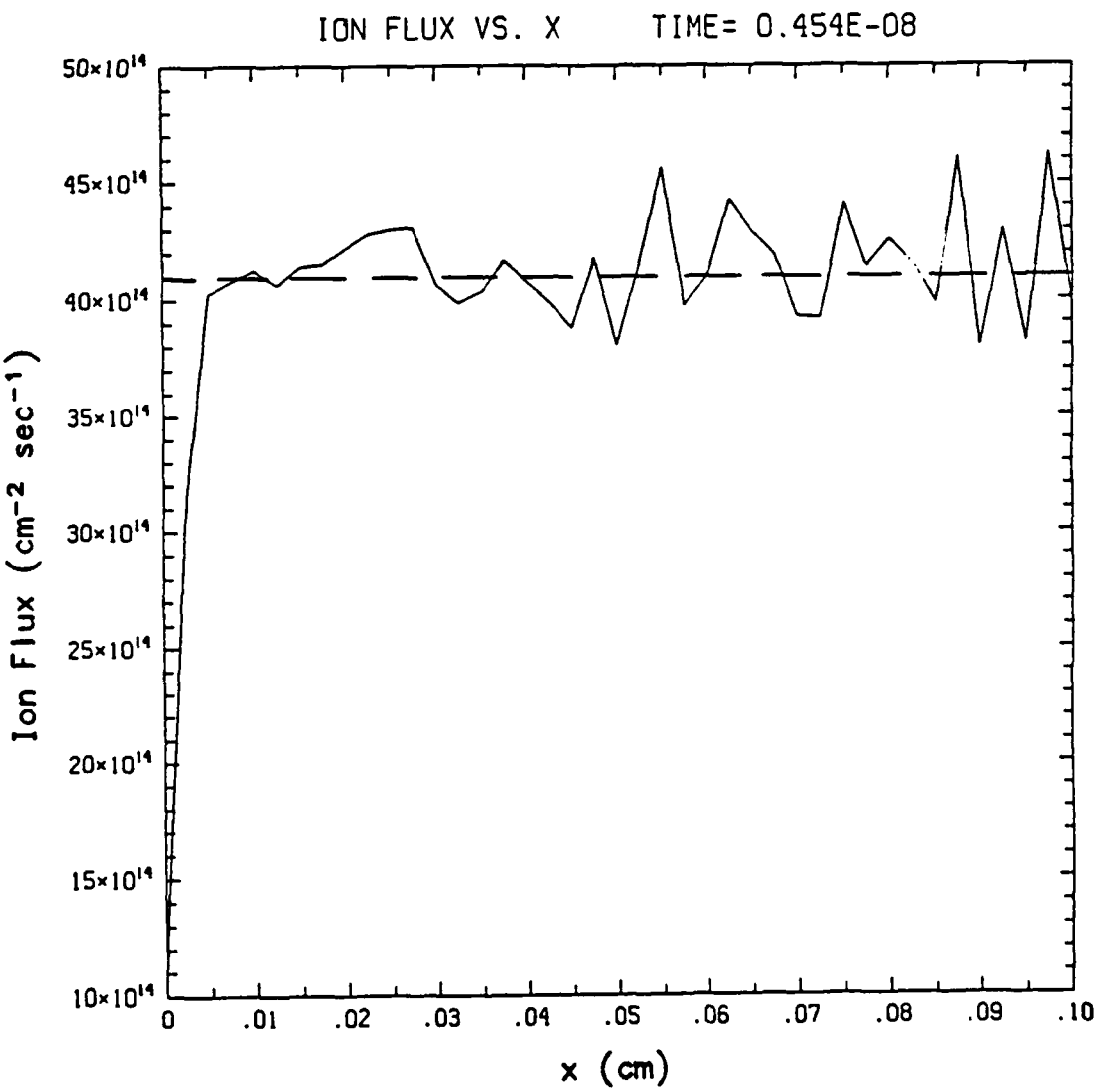

Ion Flux as a Function of x

Figure 35

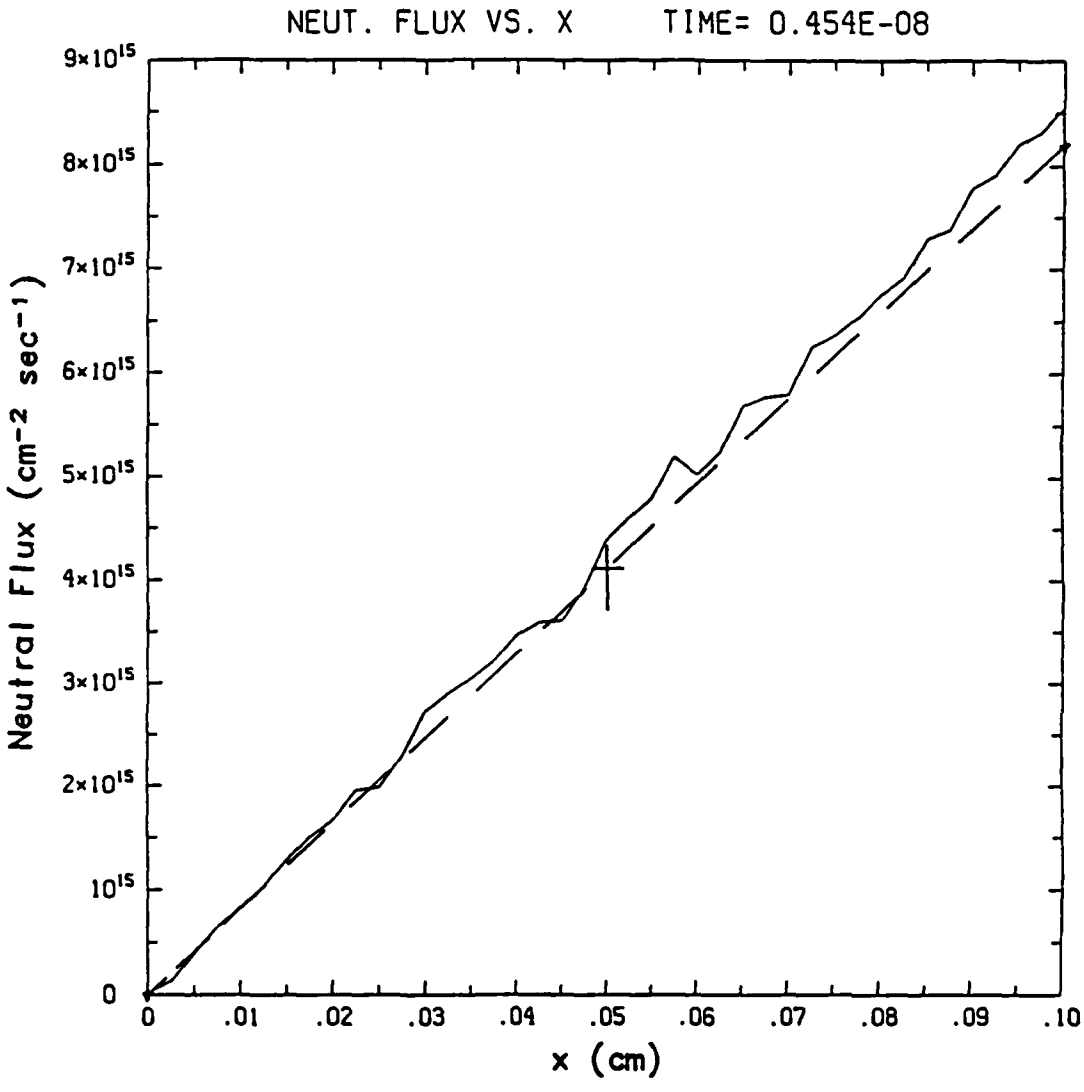

Neutral Flux as a Function of x

Figure 36

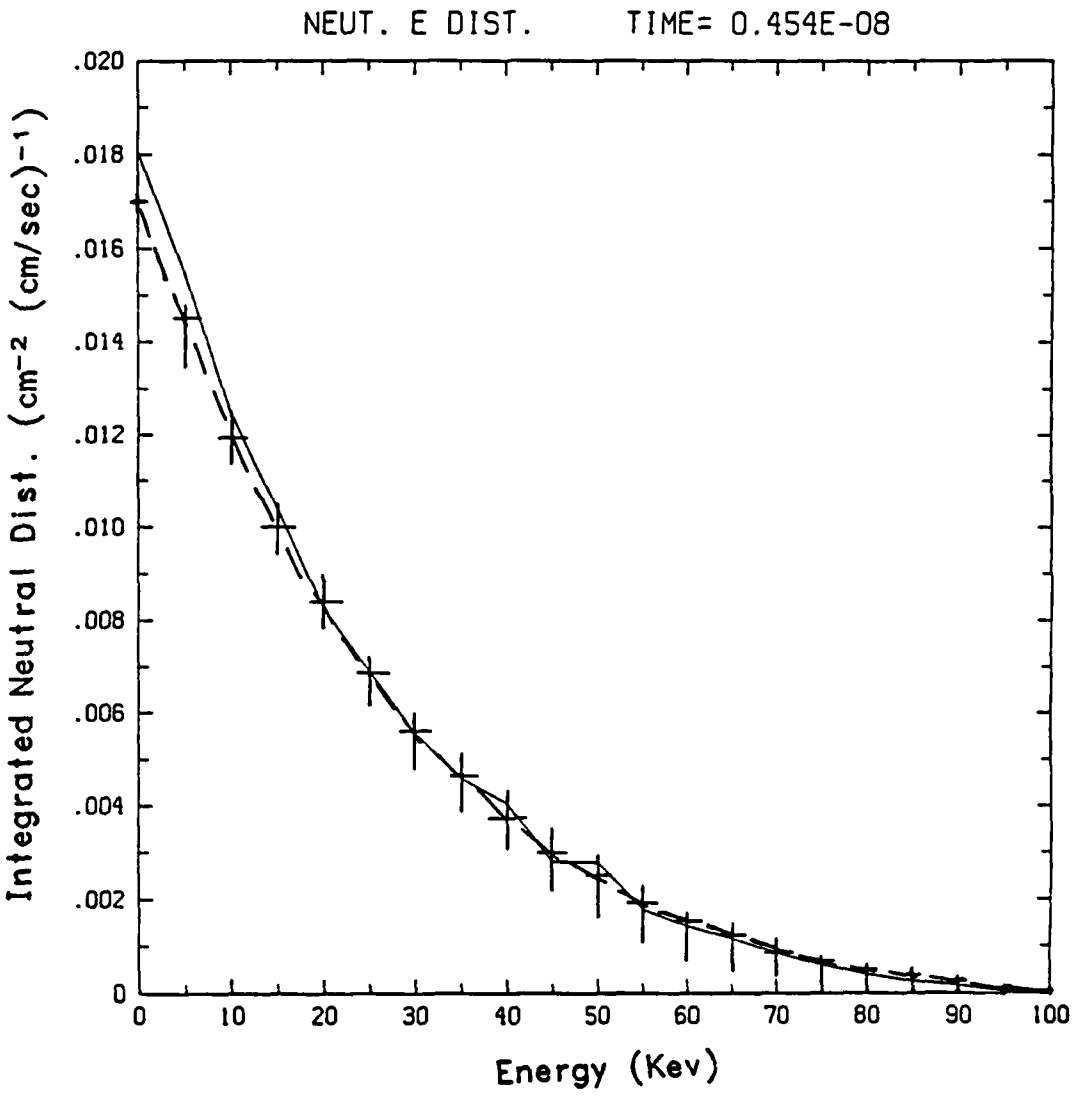

Integrated Neutral Distribution as a Function of Energy

Figure 37

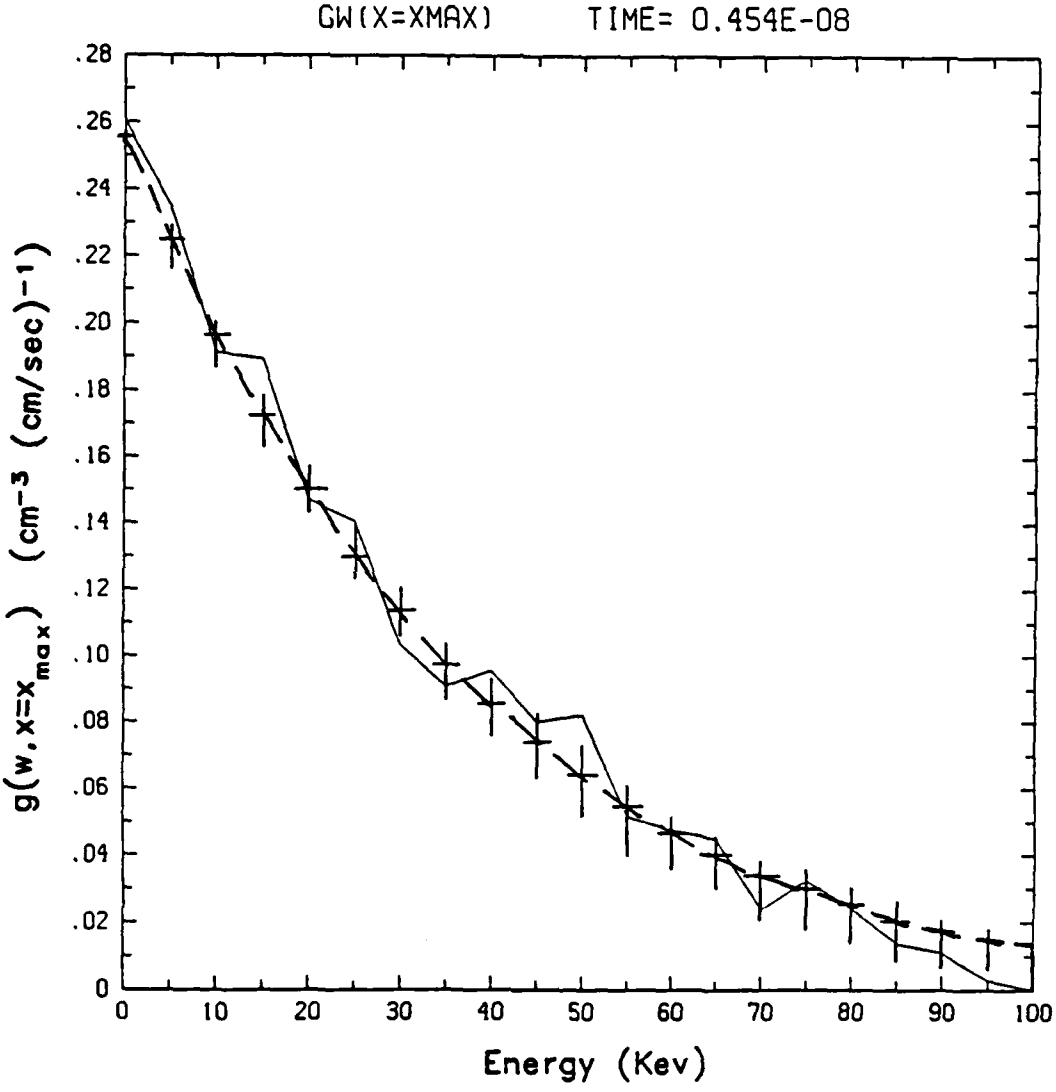

Neutral Distribution at the Vacuum Interface as a Function of Energy

Figure 38

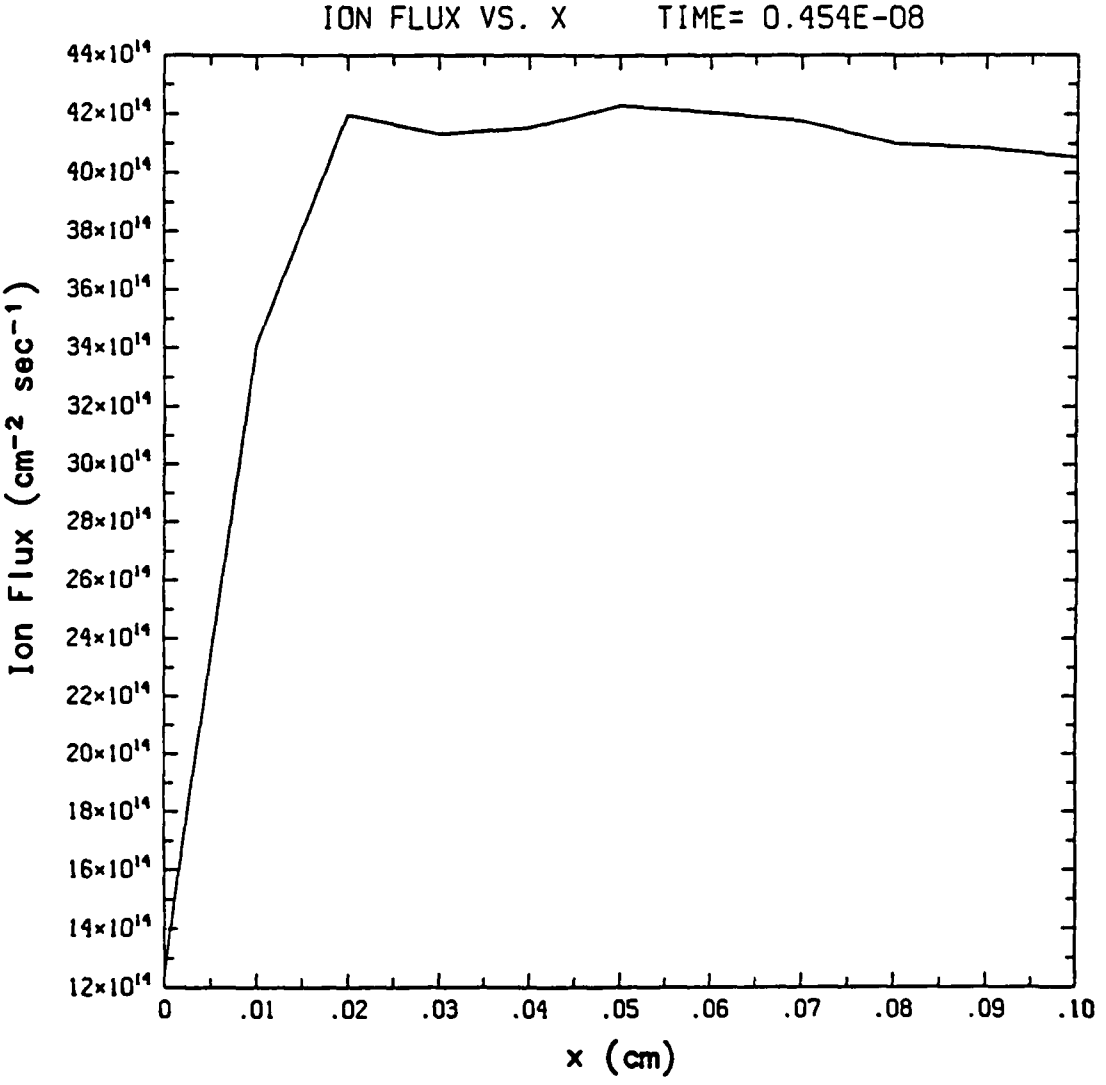

Ion Flux as a Function of x

Figure 39

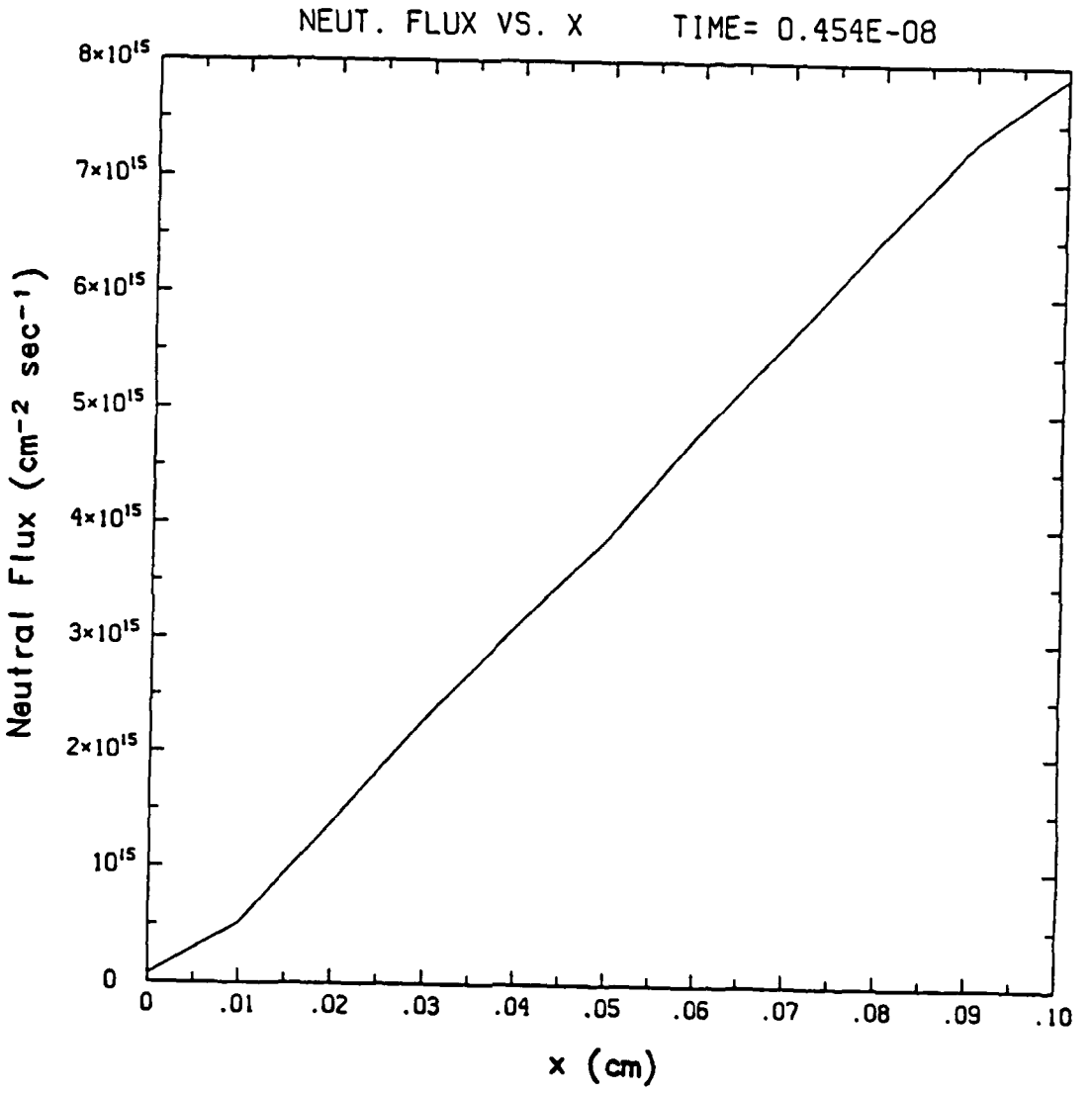

Neutral Flux as a Function of x

Figure 40

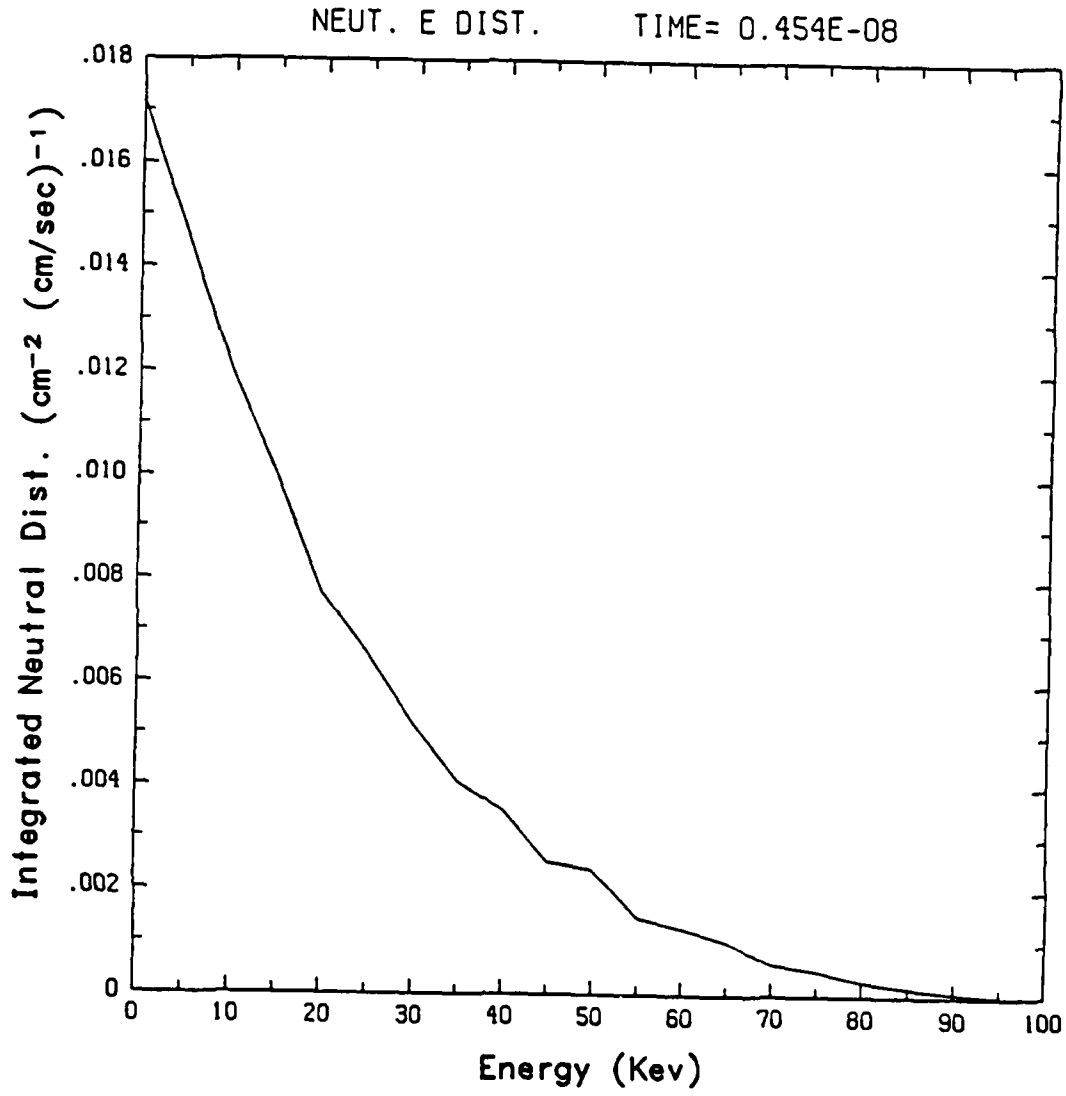

Integrated Neutral Distribution as a Function of Energy

Figure 41

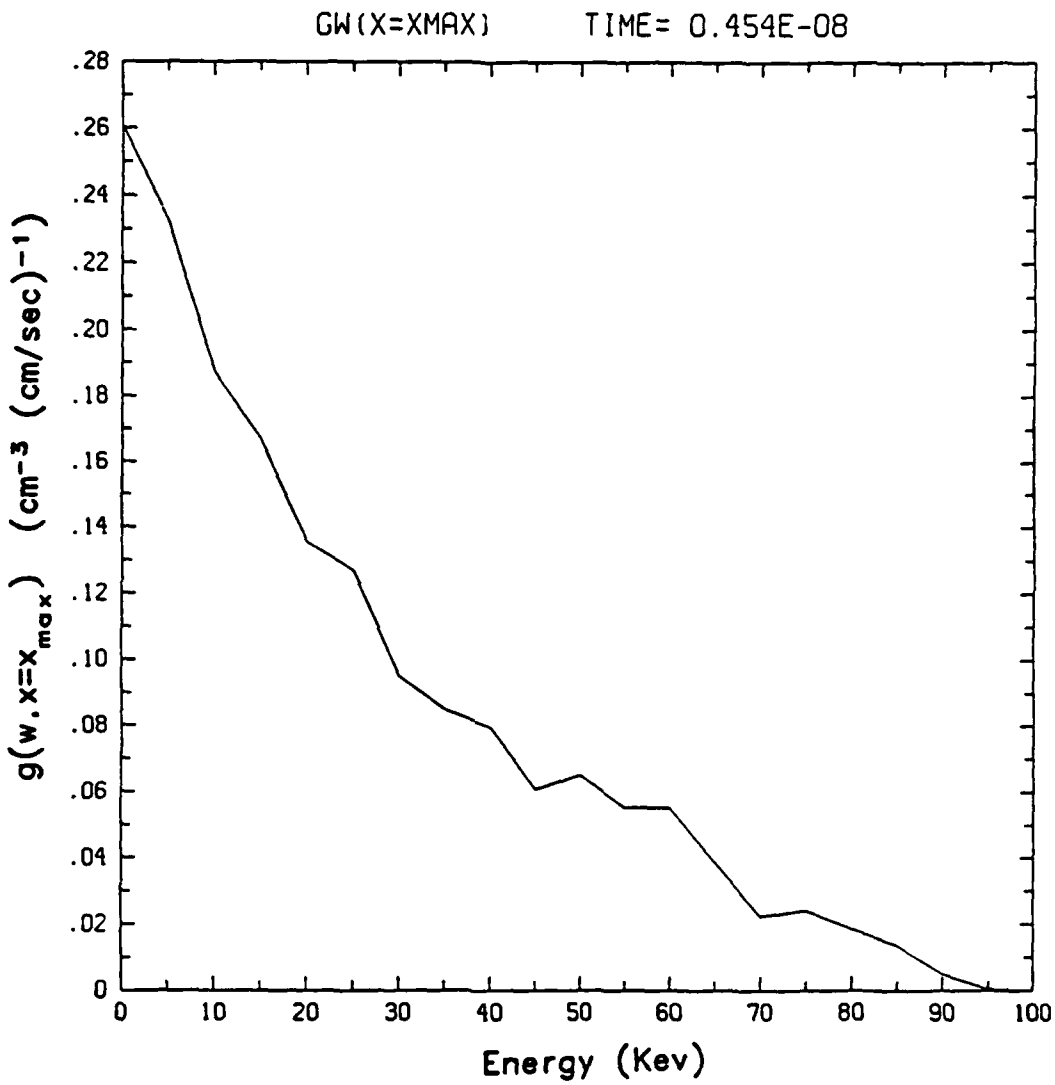

Neutral Distribution at the Vacuum Interface as a Function of Energy

Figure 42

DISTRIBUTION LIST

Assistant to the Secretary of Defense Atomic Energy Washington, D.C. 20301 Attn: Executive Assistant	1 copy
Director Defense Nuclear Agency Washington, D.C. 20305	
Attn: DDST	1 copy
TITL	4 copies
RAEV	1 copy
STVI	1 copy
Commander Field Command Defense Nuclear Agency Kirtland AFB, New Mexico 87115 Attn: FCPR	1 copy
Director Joint Strat TGT Planning Staff Offutt AFB Omaha, Nebraska 68113 Attn: JLKS	1 copy
Undersecretary of Defense for RSCH and ENGRG Department of Defense Washington, D.C. 20301 Attn: Strategic and Space Systems (OS)	1 copy
Deputy Chief of Staff for RSCH DEV and ACQ Department of the Army Washington, D.C. 20301 Attn: DAMA-CSS-N	1 copy
Commander Harry Diamond Laboratories Department of the Army 2800 Powder Mill Road Adelphi, Maryland 20783	1 copy each
Attn: DELHD-N-NP	
DELHD-TA-L (Tech. Lib.)	
U.S. Army Missile Command Redstone Scientific Information Center Attn: DRSMI-RPRD(Documents) Redstone Arsenal, Alabama 35809	3 copies
Commander U.S. Army Nuclear and Chemical Agency 7500 Backlick Road Building 2073 Springfield, Virginia 22150 Attn: Library	1 copy

Lockheed Missiles and Space Company, Inc. — 1 copy each
Post Office Box 504
Sunnyvale, California 94086
Attn: S. Taimlty
J.D. Weisner

Maxwell Laboratory, Inc. — 1 copy ea.
9244 Balboa Avenue
San Diego, California 92123
Attn: A. Kolb
K. Ware

McDonnell Douglas Corporation — 1 copy
5301 Bolsa Avenue
Huntington Beach, California 92647
Attn: S. Schneider

Mission Research Corporation — 1 copy each
Post Office Drawer 719
Santa Barbara, California 93102
Attn: C. Longmire

Mission Research Corporation-San Diego — 1 copy
5434 Ruffin Road
San Diego, California 92123
Attn: Victor J. Van Lint

Northrop Corporation — 1 copy
Northrop Research & Technology Center
1 Research Park
Palos Verdes Peninsula, California 90274

Physics International Company — 1 copy each
2700 Merced Street
San Leandro, California 94577
Attn: C. Deeney
T. Nash

R and D Associates — 1 copy each
Post Office Box 9695
Marina Del Rey, California 90291
Attn: Library

Science Applications, Inc. — 1 copy
10260 Campus Point Drive
Mail Stop 47
San Diego, California 92121
Attn: R. Beyster

Commander
Naval Intelligence Support Center
4301 Suitland Road, Bldg. 5
Washington, D.C. 20390
Attn: NISC-45

1 copy

Commander
Naval Weapons Center
China Lake, California 93555
Attn: Code 233 (Tech. Lib.)

1 copy

Officer in Charge
White Oak Laboratory
Naval Surface Weapons Center
Silver Spring, Maryland 20910
Attn: Code R40
Code F31

1 copy each

Weapons Laboratory
Kirtland AFB, New Mexico 87117-6008
Attn: Dr. William Baker
SUL
CA

1 copy each

Deputy Chief of Staff
Research, Development and Accounting
Department of the Air Force
Washington, D.C. 20330
Attn: AFRDQSM

1 copy

Commander
U.S. Army Test and Evaluation Command
Aberdeen Proving Ground, Maryland 21005
Attn: DRSTE-EL

1 copy

Auburn University
Department of Physics
Attn: Dr. J. Perez
Auburn, Al 36849

1 copy

BDM Corporation
7915 Jones Branch Drive
McLean, Virginia 22101
Attn: Corporate Library

1 copy

Berkeley Research Associates
Post Office Box 983
Berkeley, California 94701
Attn: Dr. Joseph Workman

1 copy

Berkeley Research Associates — 1 copy each
Post Office Box 852
5532 Hempstead Way
Springfield, Virginia 22151
Attn: Dr. Joseph Orens

Boeing Company — 1 Copy
Post Office Box 3707
Seattle, Washington 98134
Attn: Aerospace Library

General Electric Company - Tempo — 1 Copy
Center for Advanced Studies
816 State Street
Post Office Drawer QQ
Santa Barbara, California 93102
Attn: DASIAC

Institute for Defense Analyses — 1 copy
1801 N. Beauregard Street
Alexandria, Virginia 22311
Attn: Classified Library

JAYCOR — 1 copy
1608 Spring Hill Road
Vienna, Virginia 22180
Attn: R. Sullivan

JAYCOR — 1 copy
11011 Forreyane Road
Post Office Box 85154
San Diego, California 92138
Attn: E. Wenaas
F. Felber

KAMAN Sciences Corporation — 1 copy each
Post Office Box 7463
Colorado Springs, Colorado 80933
Attn: Library

Lawrence Livermore National Laboratory — 1 copy each
University of California
Post Office Box 808
Livermore, California 94550
Attn: DOC CDN for 94550
DOC DCN for L-47 L. Wouters
DOC CDN for Tech. Infor. Dept. Lib.

Science Research Laboratory
1150 Ballena Blvd., Suite 100
Alameda, California 94501
Attn: M. Krishnan

Spectra Technol, Inc., 1 copy
2755 Northup Way
Bellevue, Washington 98004
Attn: Alan Hoffman

Spire Corporation 1 copy
Post Office Box D
Bedford, Massachusetts 07130
Attn: R. Little

Director 1 copy
Strategic Defense Initiative Organization
Pentagon 20301-7100
Attn: T/IS Dr. Dwight Duston

Texas Tech University 1 copy
Post Office Box 5404
North College Station
Lubbock, Texas 79417
Attn: T. Simpson

TRW Defense and Space Systems Group 1 copy
One Space Park
Redondo Beach, California 90278
Attn: Technical Information Center

Naval Research Laboratory
Radiation Hydrodynamics Branch
Washington, D.C. 20375
Code 4720 - 50 copies
4700 - 26 copies
Do NOT make labels for
Records-----(01 cy)
Code 4828---(22 cys)

Director of Research
U. S. Naval Academy
Annapolis, MD 21402
(2 copies)

Naval Research Laboratory
Washington, DC 20375-5000
Code 4830
Timothy Calderwood

Naval Research Laboratory
Washington, DC 20375-5000
Code 1220